

University of Hradec Králové
Faculty of Science
Department of Physics

Stochastic properties of ionosphere as earthquake precursor

Diploma Thesis

Author: RNDr. Jan Šlégr, Ph.D.
Study Programme: N1701/Physics
Field of Study: 1701T053/Physical measurements and modeling
Thesis Supervisor: Mgr. Filip Studnička, Ph.D.

Declaration

I hereby certify that this diploma thesis is entirely the result of my own work and I have faithfully and properly cited all sources used in the thesis.

Hradec Králové, May 30, 2016

.....

Anotace

ŠLÉGR, Jan. *Stochastické vlastnosti ionosféry jako prekurzor zemětřesení*. Hradec Králové: Přírodovědecká fakulta Univerzity Hradec Králové, 2016. 47 s. Diplomová práce.

Spodní část ionosféry známá jako D-vrstva má vlastnosti gaussovsky náhodné plochy ovlivňující šíření velmi dlouhých vln. To se projevuje změnou stochastických vlastností odražených vln, protože jejich autokorelační funkce (ACF) v čase je Besselova funkce prvního druhu a nultého řádu. V této práci je testována hypotéza, že vlastnosti této Besselovy funkce jsou spojeny se seismickou aktivitou v oblasti šíření vln.

Klíčová slova:

prekurzory zemětřesení, ionosféra, autokorelace

Annotation

ŠLÉGR, Jan. *Stochastic properties of lower ionosphere as earthquake precursor*. Faculty of Science, University of Hradec Králové, 2016. 47 pp. Diploma thesis.

Lower portion of the ionosphere known as the D-layer has properties of Gaussian random plane affecting very low frequency waves. This is manifested by stochastic properties of reflected VLF waves as their auto-correlation function (ACF) in time is the Bessel function of the first kind and zero order. In this thesis the hypothesis that the properties of this Bessel function are connected with the seismic activity in the area near the great circle path of VLF waves is tested.

Keywords:

earthquake prediction, ionosphere, auto-correlation

Acknowledgements

I am profoundly indebted to my supervisor, dr. Filip Studnička, who was very generous with his time and knowledge and provided insightful discussions about the research. I also want to express my gratitude to my colleague Kamila Váňová, MSc., for help with data analysis.

This thesis was supported by the SV PřF UHK nr. 2119/2015.

Contents

Introduction	8
1 Theoretical background	9
1.1 Ionosphere – normal and irregular	9
1.2 Ionosphere content	12
1.3 Precursory effects in D-Layer of ionosphere	13
1.4 Propagation of VLF signals in D-region of ionosphere	17
1.5 Properties of VLF signals reflected by the ionosphere	19
2 Aim of the work	23
3 Methodology and methods of research	24
3.1 Measuring technique	24
3.2 Data analysis	29
4 Results	30
4.1 Other dynamic phenomena that could influence ACF	38
4.1.1 Solar flares	38
4.1.2 Magnetic storms	39
Conclusion	42
References	43
Annex A – Paper published in Journal of Seismology	I

Introduction

The classical approach to seismic prediction was based on the so-called seismic cycle implying the periodical storing and release of the seismic stress taking into account the continuous tectonic plane movement. These comparatively simple conceptions were recently reconsidered from the point of view of the fast developing theory of fractals and chaos (Bak et al. 1988). The conception of self-organizing complex systems was put forward and described in the monograph by Rundle et al. (2000).

It was shown that by Scholz et al. (1973) that the earthquake preparation process is connected with complex chain of physical and chemical transformations within the Earth's crust in the environs of the epicentre. The basis of this approach relies on dilatation theory regarding crack formation within the Earth's crust and finally the formation of the main fault in the process of shallow earthquakes preparation. These processes are accompanied by measurable changes in several physical parameters, such as concentration of radon gas, electric resistivity or geoelectric potentials. These physical quantities are then regarded as *earthquake precursors*.

In this work the properties of ionosphere over the earthquake preparation zone are studied. It will be shown that the penetration of electric field of seismic source increases the electron density in the ionospheric D-region. This process alters the stochastic properties of the ionosphere, which acts as the Gaussian random plain for the reflection of the very low frequency (VLF) waves thus altering the properties of reflected waves. Receiving of VLF waves with frequencies in range of 10-80 kHz is very easy task and can be done with minimal cost. The data analysis of auto-correlation of registered VLF signals is carried out to show the link between earthquake in the area crossing the signal path of the VLF waves and changes in auto-correlation function of the VLF signal days prior the earthquake.

1 Theoretical background

In this chapter the essential theoretical foundations are laid out. Fundamental properties of the ionosphere and its composition are studied with special focus on the D-layer. Then the precursory effects in D-layer are discussed shortly. Last part contains essential information on the propagation of VLF waves in the D-region of ionosphere.

1.1 Ionosphere – normal and irregular

The ionosphere had been defined by Plendl (1932) as a part of the upper atmosphere of Earth, which stretches from 50 km to about 500-600 km. This region is filled with ionized gas, called *plasma*. The upper bound of the ionosphere is determined as the altitude at which the concentration of charged particles of plasma, the electrons and ions, exceeds that of neutral molecules and atoms. At these altitudes the ionosphere transforms continuously into the magnetosphere, which consists of only strongly ionized plasma (i.e., in the absence of neutral molecules and atoms) and strong ambient electric and magnetic fields. The ionosphere is rising as the result of the influence of solar ionized waves and high-energy particles on different gases in Earth's atmosphere (King 1965). The structure and properties of the ionosphere depend essentially on processes occurring in the sun (called *solar activity*), on variations of Earth's magnetic field (called the *geomagnetic field effect*), movements of neutral "wind" in the upper atmosphere due to Earth's rotation, on the effects of electrical current and ambient electrical field, on the density and the content of the atmosphere at different altitudes and geographical latitudes, and so on.

Usually, the ionosphere is separated into five independent regions, sometimes called layers (Ratcliffe, 1960, see Fig. 1). The bottom one, from 50 to 80 km, is called the D layer, from 80 to 130 km is the E layer, and above 150 km is the F layer. The latter region is usually separated at the F₁ layer, from 130 to 200-250 km, and the F₂ layer is above 250 km. Apart from these layers, at 90-120 km, the sporadic layer E is observed, whose thickness in the vertical plane along the height is small. Its occurrence is usually explained by the influence of a neutral wind of atmospheric gases on the charged particles of plasma, resulting in exchange of plasma accompanied by stratified wind structure along the height (for more detailed information, see Ratcliffe, 1956).

Historically, the division arose from the successive plateaus of electron density (N_e)

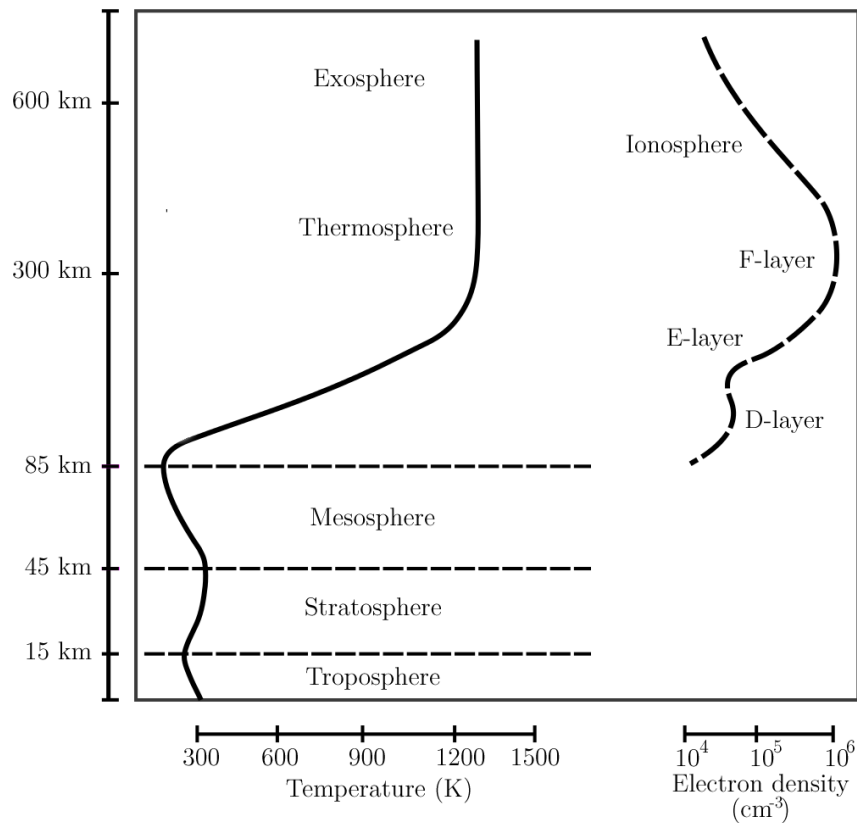


Figure 1: Layers of atmosphere and ionosphere according to Ratcliffe (1960)

observed on records of the time delay (i.e., virtual height) of radio reflections as the transmitted signal was swept through frequency. (The critical frequency at which reflection occurs varies as N_e . Thus higher frequencies penetrate farther into the ionosphere and are reflected by higher N_e) The E "layer" was the first to be detected and was so labeled as being the atmospheric layer reflecting the **E** vector of the radio signal. Later the lower D and higher F layers were discovered. Distinct ionospheric regions develop because

- the solar spectrum deposits its energy at various heights depending on the absorption characteristics of the atmosphere,
- the physics of recombination depends on the density, and
- the composition of the atmosphere changes with height.

Thus the four main ionospheric regions can be associated with different governing physical processes, and this physics (rather than simple height differentiation) is the basis for labeling an ionospheric region as a D, E, F₁, or F₂ region.

At altitudes lower than 75 km the negative ion concentration prevails over the electron concentration. Due to the NO reaction extinction in winter the electrons concentration grows, that's why the electron density is higher in the D-region during the winter days than in the summer. The diurnal variations of electron concentration in the D-region (difference between the noon and midnight values) can reach 1.5 orders of magnitude for low solar activity and 2.5 orders for periods of high solar activity.

Now, taking into account the geomagnetic line structure as well as the irregular distribution of variations of the geomagnetic field above Earth and its influence on the ionosphere, the latter can be categorized as the high-latitude ($|\Phi| > 55^\circ - 60^\circ$), middle-latitude ($30^\circ \leq |\Phi| \leq 55^\circ$), and lower-latitude ($|\Phi| < 30^\circ$) ionosphere, with a special zone of geomagnetic equator with $|\Phi| \leq 5^\circ - 10^\circ$, where Φ is the magnitude of the geomagnetic latitude (Ratcliffe, 1960). Note that in the physics of magnetosphere-ionosphere interactions, the definition "geomagnetic latitudes" relates to the dipole distribution of Earth's magnetic field when the magnetic dipole is located at the center of Earth and the magnitude of $\Phi = \tan^{-1}(\frac{1}{2}\tan I)$, where I is the angle of the magnetic field inclination.

These processes are source of plasma instabilities generated in the irregular ionosphere. There is a wide spectrum of small-, moderate-, and large-scale natural plasma structures (turbulences) observed experimentally in the ionosphere at different altitudes, covering all regions from the equator to the polar cap.

Heating-induced plasma irregularities can be generated by local heating of the ionosphere with powerful radio waves, which finally generates parametric and striction instabilities in plasma. The same effects can be observed in the ionosphere in other natural conditions, so that non-isothermal conditions occur in the ionospheric plasma during heating of plasma particles by electric fields (due to fluctuations of the ambient electric field as a local heater of ionospheric plasma). According to Blaunstein and Plohotniuc (2008), plasma instabilities can also be generated by the wind of neutral molecules (atoms), by drift in crossing ambient electrical and magnetic fields (usually denoted as $\mathbf{E} \times \mathbf{B}$ drift), and by other current-induced two-stream instabilities. At the same time, most natural small-, moderate-, and large-scale plasma structures observed experimentally in the auroral and equatorial ionosphere can be explained by the existence of plasma waves caused by convergent-current and gradient-current instabilities. All these phenomena can be unified as the natural sources of plasma instabilities in

the regular ionosphere, altering significantly the properties of the ionosphere for radio wave propagation.

Heating-induced (or thermal) and current-induced instabilities as the main sources of the small-, moderate-, and large-scale plasma density perturbations, δN , which can be either positive or negative compared to non-disturbed background ionospheric plasma density N . Usually, a case in which $\delta N > 0$ is called *plasma density enhancements*, and one in which $\delta N < 0$ is called *plasma density depletions*.

The gradient-drift instability generates long-length perturbations (e.g., waves) with wavelengths of 100 m and more, up to 10 km, when the diffusion relaxation process (which usually decreases growth of such instabilities) is sufficiently weak. Such large-scale plasma perturbations generate small-scale secondary gradient-drift waves propagating at large flow angles to the ambient $\mathbf{E}_0 \times \mathbf{B}_0$ drift. Thus, the nonlinear cascade wave interactions can be assumed to be the main mechanism of generation of small-scale plasma irregularities usually observed in the equatorial ionosphere

On the other hand, plasma perturbations (i.e., waves) of a large range of scales, from tens to hundreds of kilometres creating diffuse-spread traces observed by ionosondes in the middle-latitude ionosphere (see Bowman, 1991), are evidence of a complicated non-linear mechanism of plasma waves interaction.

1.2 Ionosphere content

The neutral atmosphere in conditions of hydro-static equilibrium and in the isothermal case ($T_m(z) = const$, where z is the altitude of the atmosphere from Earth's surface), the deviation of concentration of the neutral molecules and atoms in the ionosphere along height z is described by the barometric formula:

$$N_m = N_{m0} \exp\left(-\frac{z - z_0}{H_m}\right) \quad (1)$$

where $N_m = \sum_{\beta} N_{\beta}$, where β is the type of neutral particle; N_{m0} is the concentration of neutral particles at the height $z = z_0$ of pressure equilibrium; and $H_m = T/M_m g$ is the height of the homogeneous atmosphere, where $T = T_m$ is the temperature of neutral particle content in energetic units, $M_m = \sum_{\beta} m_{\beta} N_{\beta} / N_m$ and g is the gravitational acceleration ($g = 9.81 \text{ m} \cdot \text{s}^{-2}$, and m_{β} is the mass of the particle β).

Equation (1), as with all macroscopic gas laws, is valid for the ionosphere only under conditions such that the number of interactions between atoms and molecules is

sufficient to establish a statically physical balance between them. In the case of Earth's ionosphere, equation (1) is valid up to altitudes of $z_e \approx 1000 - 1200$ km (Volland, 1984). For $z > z_e$, the length of the free path, l_β , of gas particle between interactions exceeds the height of the regular atmosphere H_m i.e., $l_\beta \gg H_m$, and neutral particles can move freely without collisions between them, and finally leave Earth's atmosphere. The region with altitude $z > z_e$, in which this phenomenon occurs, is called the exosphere (Richmond, 1995).

The D-region is characterized by the most complex ion composition. It contains the large ion clusters such as $H^+(H_2O)_n$, $NO^+(H_2O)_n$, $NO^+(CO_2)_n$ etc. It is the only region of the ionosphere where the concentration of the positive ions is not equal to the electron concentration due to formation of the negative ions. Main source of ionization is the Lyman- α radiation ($\lambda = 121.6$ nm). It can ionize the neutral atmosphere NO with very low ionizing energy and forming NO^+ ions at heights of 60 – 90 km. The hard solar and galactic X-rays ($\lambda < 1$ nm) together with energetic precipitating particles ionize the main molecular components O_2 and N_2 and solar ultraviolet radiation in the interval $102.8 < \lambda < 11.8$ nm ionize the excited oxygen molecules. For detailed information on other ionosphere layers please see Ratcliffe (1960).

1.3 Precursory effects in D-Layer of ionosphere

The complex chain of processes in the atmosphere, ionosphere, and magnetosphere results in precipitating particles producing ionization of the lower ionosphere. Earthquake preparation is accompanied by a set of precursory phenomena connected with the transformations within the Earth's crust. The *gaseous emanation* is one of the important earthquake precursors. Among different gases emanating from the crust the radon gas is able to produce air ionization (Toutain and Baurbon, 1998). The regular gas discharges, especially of CO_2 can carry with them the products of geomorphology in the form of aerosols including high metal content aerosols. The metals could be also emanated from the crust in form of volatile metals such as Hg, As and Sb (Klusmand 1993). These metallic aerosols could be easily charged and therefore change the electrical properties of the air near the ground. The last important phenomenon is the *anomalously large vertical electric field* registered in the earthquake preparation zone several days or hours before the seismic shock (Hao et al. 2000).

The ionization leads to an increase in the electron concentration in the D-region of

the ionosphere which is equivalent to lowering the ionosphere (Kim et al. 2002). This lowering changes the condition of radio wave propagation in different frequency bands from VLF up to VHF.

In a stationary state that assumes, in particular, the absence of particle drift, the concentration of different plasma species along the geomagnetic field line is determined by the partial balance of the pressure, gravity and the longitudinal (along the ambient geomagnetic field) polarization electric field forces. It is possible to seek for the effects of the seismogenic electric field on the ion balance along the magnetic tube solving the continuity equation. This problem was treated by Shklyar and Truhlik (1998). In the simplified model approach (only two ion species, isothermal ionosphere, neglecting of the geomagnetic field line curvature) they analysed the ion balance within the magnetospheric tube affected by the electric field of seismic origin perpendicular to the geomagnetic field line. This arrangement exactly coincides with the field configuration regarded by Kim and Hegai (1997) for the upper ionosphere. Shklyar and Truhlik (1998) demonstrated the high sensitivity of the light ions to the changes in the background ionosphere. This means that the slight local changes in the base of the magnetic tube caused by the particle drift under the action of electric field lead to the strong changes of light ion concentration.

To calculate the rate of collisional ionization of the neutral atmospheric components by precipitating energetic electrons we can apply the calculation technique developed in Rees (1963). According to his paper, the rate q of creation of ion pairs in a unit volume, normalized to the monoenergetic flux F of electrons with energy E_0 is given by the formula:

$$\frac{q}{F} = q(E_0)(e) = \frac{E_0}{r_0 \Delta E_{ion}} \lambda \left(\frac{z}{R} \right) \frac{n(M)_z}{n(M)_R}$$

where $\Delta E_{ion} = 0.035$ keV is the ionization energy per ion pair, $r_0 = R/\rho$, ρ is the air density at the maximum depth R to which electrons with a given energy can penetrate, $\lambda(z/R)$ is the dimensionless distribution function of energy loss and

$$z = \int_h^{h_{top}} \rho dh$$

where h is the height in the atmosphere at which the ionization rate is calculated, $h_{top} = 1,000$ km is the adopted altitude of the upper boundary of the atmosphere, and $n(M)_z$ and $n(M)_R$ are the number densities of atoms and molecules being ionized at depths z and R , respectively. In this case, the maximum depth of penetration into

the atmosphere and the initial electron energy $0.4 \text{ keV} \leq E_0 \leq 500 \text{ keV}$ at the upper boundary of the atmosphere are related as follows: $R [\text{g}/\text{cm}^2] = 4.57 \cdot 10^{-6} (E_0 [\text{keV}])^{1.75}$. If the flux of precipitating electrons having an arbitrary differential energy spectrum $g(E_0)$ in the energy range from E_0^{min} to E_0^{max} is isotropic over the upper hemisphere, then the ionization rate Q per unit volume can be presented in the following way:

$$Q = \pi \int_{E_0^{min}}^{E_0^{max}} g(E_0) q_{E_0}(e) dE_0.$$

It is known that the electron density in the night-time ionospheric D-region before a severe earthquake can significantly increase (Pulinets 2004). This effect is most pronounced if a powerful VLF radio station operates in the vicinity of the epicentral zone of an earthquake under preparation. In this case, a fairly pronounced, dense ionized layer with maximum electron density about $2 \cdot 10^4 \text{ cm}^{-3}$ is formed in the nighttime upper mesosphere at an altitude of about 85 km. The disturbed electron density exceeds the background values by more than one order of magnitude at altitudes 85-90 km and by 2 and 3 orders of magnitude at altitudes of 75 and 85 km, respectively. And concentration still remains higher than 10^3 cm^{-3} for $h > 73 \text{ km}$. In regions far away from the operating VLF radio stations, the earthquake precursors in the nighttime D-region are less pronounced. The effect of increasing concentration in the D-region is equivalent to the effective lowering of the ionosphere. Such lowering was detected also as a result of particle precipitation due to thunderstorm activity in California (Rillekrug 2003).

One of the first experimental results concerning the D-layer reaction on the earthquake preparation was the change of the parameters of VLF signals received by ground-based receivers from remote transmitters, mainly from the Omega navigational transmitters (10.2-13.6 kHz) (Gokhberg et al. 1987). The amplitude and phase distortions of the received signal were interpreted as influence of the waveguide earth-ionosphere where the VLF signal propagates. It was proposed that the distortions are due to ionosphere lowering over the region of the earthquake preparation. It was believed that by triangulation it would be possible to determine the position of the future epicentre, and from the distortions amplitude to determine the earthquake magnitude. The time of the earthquake had a relation with the time of the VLF signal anomalies appearance. As a result, the registration of variations of the VLF signal parameters during its subionospheric propagation over the earthquake preparation zone was proposed for

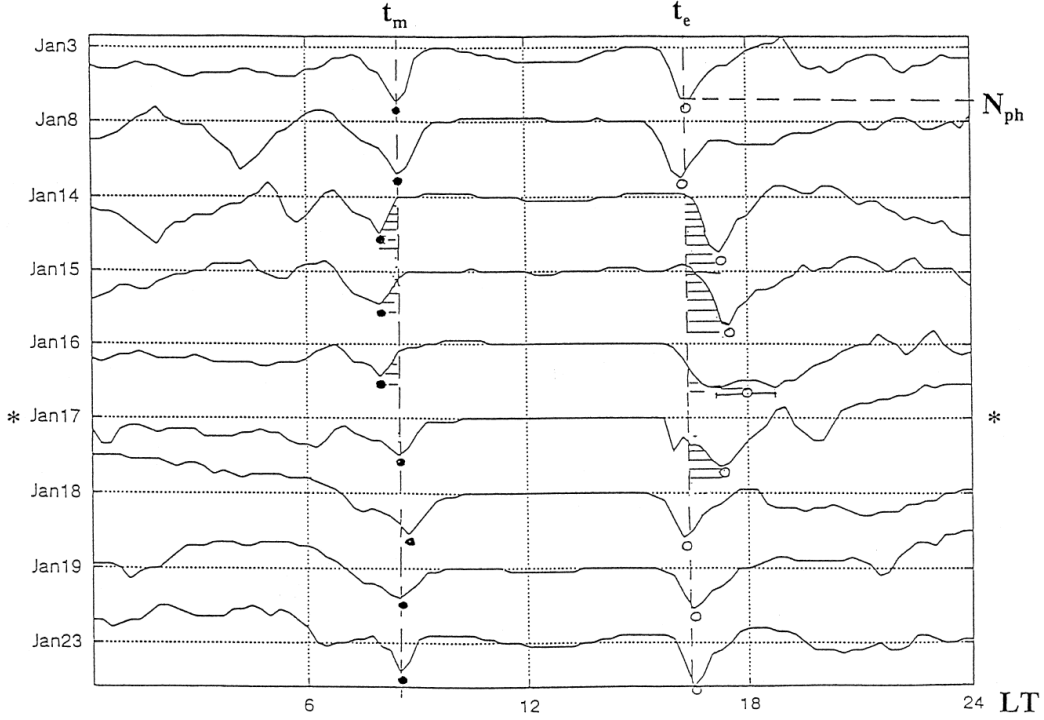


Figure 2: Sequential plots of the diurnal variation in VLF signal phase at Inubo ($f = 10.2$ kHz). The whole scope of registration is 100 centicycles. The definitions of t_m and t_e are given as the times where a minimum in phase takes place around sunrise and sunset, respectively. The value of phase at the phase minimum is defined as N_{ph} . It is seen that abnormal behaviour in the diurnal variation begins a few days before the earthquake (17 January) is the earthquake date indicated by a star. such that we have the lengthening of daytime conditions that is found to last for a few days even after the earthquake.

short-term earthquake prediction (Gufeld et al. 1994).

This technique was modified later to apply it in Japan (Hayakawa 2001). It uses not the arbitrary fluctuations in the received VLF signal but the variations of the terminator time (sunrise and sunset) observed on the VLF phase records a few days before the earthquake (Molchanov et al. 1998a, 1998b). Examples of the records are shown in Fig. 2. This method was criticized by Cliverd et al. (1999) using the same technique at long passes from North America to Antarctica permitting to monitor the effects of the earthquakes in Southern America, but it should be noted that they used the other geometry of the signal passes in relation to the terminator orientation in comparison with the Japanese experiments which may lead to the difference in the results obtained.

Nevertheless, the investigations with VLF propagation were continued in Japan and received new interpretation connected with the AGW influence on the ionosphere (Miyaki et al. 2002) and VLF monitoring is proposed for the planetary studies of the

atmosphere-ionosphere boundary including the pre-earthquake effects.

Changes in the Earth's crust in the form of deformations, variations in seismic waves velocity, emanation of gases from the Earth's crust, changes in crustal electric conductivity, etc. are observed not only at the earthquake source but also in the zone exceeding the source dimensions by an order of magnitude. This made it possible to develop a dilatation theory - deformation of the Earth's crust, fracturing, and formation of a main fault in the so-called earthquake preparation zone (Scholz et al. 1973). The dimensions of this zone were estimated by Dobrovolsky et al. (1979), based on calculating the Earth's crust elastic deformation and can be presented in the form:

$$\rho = 10^{0.43M} \text{ km},$$

where ρ is the radius of the earthquake preparation zone, and M is the magnitude. Although a dilatation theory is valid only for shallow earthquakes, and prognostic papers now are based on the statistical processing of seismic data, the use chaos theory and self-organized criticality (Kossobokov et al. 2000), the dimensions of the preparation zone determined statistically by modern theories are of the same order of magnitude as older determinations of Dobrovolsky et al. (1979).

The penetration of electric field of seismic source into the plasmasphere causes formation of a VLF duct. Inside this duct cyclotron-resonance interaction between waves and particles leads to precipitation of energetic electrons into the lower atmosphere, finally leading to the increase in electron density in the ionospheric D-region. It was proposed that the additional electric field in the ionosphere cause the electric currents and turbulence. Heigi et al. (1997) calculated that for sufficiently strong electric field of short duration very anisotropic disturbances emerges with much longer duration than primary pulse of the electric field.

1.4 Propagation of VLF signals in D-region of ionosphere

While for many years ionosphere was regarded as uniform, homogeneous and regular-layered medium over short distances, for long propagation multidiffraction, multireflection and multiscattering effects are observed due to the formation of natural and artificial plasma structures. Received waves then arrives at receiver via several paths, thus the various waves arrive with different time delays and combine vectorially to give an oscillating signal (see fig. 7 for typical VLF signal for the long propagation path).

These signal amplitude random variations are known as the fading effect. There are two main types:

- Slow fading, which is caused by diffraction from small-scale plasma structures,
- Fast fading, which is caused by the mutual interference of the wave components of the multiray field.

These effects are observed for propagation paths of about half or one wavelength (roughly 700 to 1 500 km for VLF signal at 20 kHz). The signal received in any given point may consist of large number of signals having randomly distributed amplitudes, phases, and angles of arrival, as well as different time delays. All these features change the relative phase and amplitude of the received signal, summing vectorially with the line-of-sight signal.

Rayleigh fading is commonly used to describe the fast fading. As is well known (Rappaport, 1996), a Rayleigh distribution can be obtained mathematically as the limit envelope of the sum of two Gaussian noise signals. In practice, this distribution takes place in wireless communication if each multipath component of the received signal is independent and if the phases of multipath components are uniformly distributed over the range $(0, 2\pi)$. Then, we may deal with Rayleigh distribution of random variable x , the probability density function of which can be presented in the following form (Rappaport, 1996):

$$PDF(x) = \frac{x}{\sigma^2} \exp -\frac{x^2}{2\sigma^2} \text{ for } x \geq 0.$$

As was mentioned earlier, usually in ionospheric communication, it is not only multipath component that arrive at the receiver due to multiple reflection, diffraction and scattering from various plasma obstructions along the propagation path. A line-of-sight component describing signal loss along the path of direct visibility (called the dominant path) between both antennas is often found. This dominant component of the received signal may significantly decrease the depth of the interference picture of the signal envelope variations. The PDF of such a signal is said to be Rician.

The Rician probability function distribution of the signal strength or voltage denoted by arbitrary random variable x , can be defined as (Rappaport, 1996)

$$PDF(x) = \frac{x}{\sigma^2} \exp \left(-\frac{x^2 + A^2}{2\sigma^2} \right) \cdot I_0 \left(\frac{Ax}{\sigma^2} \right) \text{ for } A > 0, x \geq 0,$$

where A denotes the peak strength or voltage of the dominant component envelope and I_0 is the modified Bessel function of the first kind and is zero-order.

1.5 Properties of VLF signals reflected by the ionosphere

The main parameter studied in this thesis is the auto-correlation of the received signal. For two random variables X and Y , the correlation is defined by

$$\text{corr}(X, Y) = \frac{\text{cov}(X, Y)}{\sigma_X \sigma_Y},$$

where σ_X denotes standard deviation and $\text{cov}(X, Y)$ is the covariance of these two variables. For the general case of variables X_i and X_j , where $i, j = 1, 2, \dots, n$,

$$\text{corr}(X_i, X_j) = \frac{\text{cov}(X_i, X_j)}{\sqrt{V_{ii} V_{jj}}},$$

where V_{ii} are elements of the covariance matrix. Correlation gives the strength of the relationship between variables. For $i = j$,

$$\text{corr}(X_i, X_i) = \frac{\text{cov}(X_i, X_i)}{\sigma_i^2} = 1.$$

Covariance is a measure of the strength of the correlation between two or more sets of random variables.

$$\text{cov}(X, Y) = \langle (X - \mu_X)(Y - \mu_Y) \rangle = \langle XY \rangle - \mu_X \mu_Y,$$

where $\mu_x = \langle X \rangle$ and $\mu_y = \langle Y \rangle$ are the respective means (Spiegel, 1992). For periodic sequence $\sum_{i=0}^{N-1} a_i$ the autocorrelation of the sequence is the sequence

$$\rho_i = \sum_{j=0}^{N-1} a_j \bar{a}_{j+i},$$

where \bar{a} denotes the complex conjugate and the final subscript is understood to be taken modulo N .

Similarly, for a periodic array a_{ij} with $0 \leq i \leq M - 1$ and $0 \leq j \leq N - 1$, the autocorrelation is the $2M \times 2N$ -dimensional matrix given by

$$\rho_{ij} = \sum_{m=0}^{M-1} \sum_{n=0}^{N-1} a_{mn} \bar{a}_{m+i, n+j},$$

where the final subscripts are understood to be taken modulo M and N , respectively (Bracewell, 1962).

As will be shown in the Part 4, received signal is scintillating – this is a consequence of the existence of random electron-density fluctuations within the ionosphere. These irregularities distort the original wavefront, giving rise to a randomly phase-modulated wave $k_0(\Delta\varphi)$, where for a radio wave of length λ , $k_0 = \frac{2\pi}{\lambda}$ is the free-space wave-number, and $\Delta\varphi$ is the variation of the optical path length within the layer with irregularities. $\Delta\varphi$ is dependent on the fluctuations of the ionospheric total electron content ΔN_T caused by irregularities:

$$\Delta\varphi = -\frac{2\pi r_e \Delta N_T}{k_0},$$

where r_e is the classical electron radius.

As the wave propagates toward the receiver, further phase mixing occurs, changing the modulation of the wave and eventually producing a complicated diffraction pattern on the ground. If the ionosphere move relative to the receiver, temporal variations of intensity and phase are recorded. Simple considerations show that the amplitude fluctuations are mainly caused by irregularities with size of the order of the first Fresnel zone $d_F = \sqrt{\lambda(z - L/2)}$, where z is the height of the upper boundary of the irregular layer, and L is the layer thickness.

This scenario of scintillation generation is valid provided $\Delta\varphi$ is not too large. If the electron density fluctuations are significant, then the phase fluctuations can be so large that the wave is no longer coherent and the interference of rays is not possible. Analysis shows that when the phase fluctuations reach a certain limiting value, the intensity of amplitude scintillation ceases to increase.

Scintillation theory relates the observed signal statistics to the statistics of ionospheric electron density fluctuations (see Yeh and Liu, 1982). The general problem of propagation of wave in a random medium is difficult to treat numerically. However, it can be greatly simplified if the wavelength is much smaller than the characteristic scale size of irregularities. In this case the wave is scattered predominantly in the forward direction and the wave propagation is described by the parabolic equation, which can be easily solved (Wernik et al., 1980). Further simplifications are possible if the irregular layer is so thin that $\sqrt{\lambda L}$ is much smaller than the size of largest irregularity contributing to scintillation. This assumption leads to the so-called phase screen theory of scintillation in which the irregular layer is replaced by a screen, which changes only the waves phase. The screen is located in the ionosphere at the height of the maximum electron density. Historically, the phase screen model was the first model of scintillation

(Hewish, 1951). Later expansion (Rino, 1982) included the geometry of propagation, anisotropy of irregularities and strong scatter case.

Knepp (1983) introduced the multiple phase screen model which let to analyse propagation of waves through a thick irregular layer with arbitrary electron density background profile.

As a measure of the scintillation intensity, the scintillation index S_4 is most often used. It is defined as a normalized variance of the signal power:

$$S_4 = \frac{\langle A^4 \rangle - \langle A^2 \rangle^2}{\langle A^2 \rangle^2}.$$

If the scintillation index at a certain frequency is known, one can infer the scintillation intensity at another frequency, provided the amplitude scintillation spectral index p_s is known. Both the theory and observations show that S_4 scales as $f_w^{-\alpha}$, where f_w is the wave frequency and $\alpha = (p_s + 3)/4$. For ionospheric scintillation, the spectral index is often close to 3, and the scintillation intensity scales as $f_w^{-\frac{3}{2}}$. Such simple scaling is justified only for not too intense scintillation. If scintillation is moderately strong or strong, the scintillation spectrum has a form close to Gaussian and it is not possible to determine the spectral index.

Two examples of amplitude scintillation, their spectra, and cumulative probability distribution functions, corresponding to weak and moderately strong conditions, are shown in Fig. 3. Data were collected from the Hilat satellite at the Polish Polar Station on Svalbard. At high frequencies, the weak-scintillation spectrum fits quite well the power-law. However, the moderately strong scintillation spectrum appears Gaussian rather than a power-law.

Fig. 3 also shows the experimental cumulative probability-density function and the best-fit log-normal density function. While, for weak scintillation, the experimental and theoretical probabilities agree satisfactorily, for strong scintillation they differ markedly. Fremouw et al. (1980) have made a thorough analysis of scintillation statistics. They concluded that the best fit to the observed amplitude and phase scintillation is obtained with a two-component model. In this model, it is postulated that the high-frequency, diffractively scattered component obeys generalized Gaussian statistics and the low-frequency, refractively focused component obeys log-normal statistics. Wernik (1997), who applied wavelet filtering to investigate the probability distribution function of scintillation at selected frequencies, later confirmed this conclusion. Phase is nearly

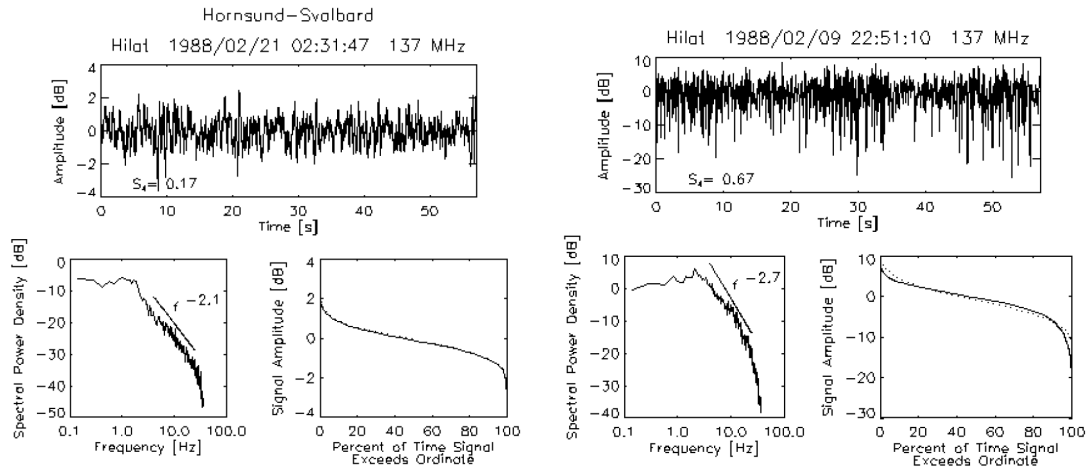


Figure 3: Examples of the amplitude scintillation, their power spectra and cumulative probability densities for weak (upper frames) and moderately strong (lower frames) scintillation. The power-law fit to each spectrum between 4 and 25 Hz is shown. The dotted line is the log-normal probability density (Wernik et al., 2003).

always normally distributed, without regard to the strength of scatter.

2 Aim of the work

Aim of the work is to demonstrate the link between the stochastic properties of lower ionosphere (the D-layer) and seismic activity. Stochastic properties are investigated by means of reflected VLF (Very Low Frequency) signals. The D-layer acts as Gaussian random plane for VLF waves reflection. Reflected waves have properties of random waves which is manifested by the fact that their auto-correlation function in time is Bessel function of second kind and it is zero-order. In this work we show that the properties of the Bessel function are connected with the seismic activity in the area near the great circle path of VLF waves.

Several ionospheric precursors of earthquakes are currently under investigation (for details see Pulinets, 2004 or Perrone et al., 2010), some of them using the VLF waves reflected by the ionosphere (Hayakawa et al., 2011). Electromagnetic precursors of earthquakes (not limited to VLF part of the electromagnetic spectrum) are discussed with case studied in recent monograph (Hayakawa, 2015).

These precursor have one common advantage – technical realisation of VLF receiver is very simple and inexpensive due to the frequency range in the tens of kilohertz. Such receivers and detectors can therefore be manufactured inexpensively and in large quantities and placed into promising areas.

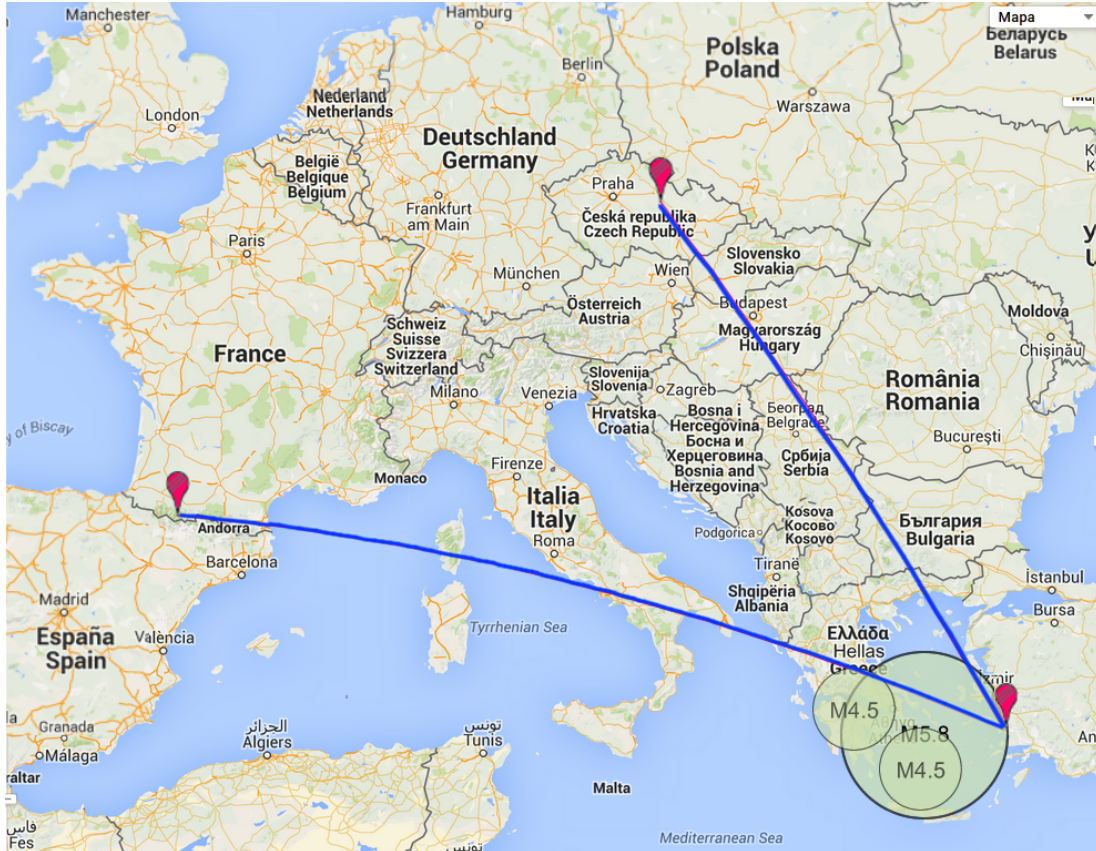


Figure 4: Great circle paths of VLF waves from TBB transmitter with the preparation zones

3 Methodology and methods of research

3.1 Measuring technique

For the survey described in this thesis the Denizköy VLF transmitter located in Turkey ($37^{\circ}24'43''N$ $27^{\circ}19'25''E$) active on 26700 Hz under the call-sign TBB was chosen. Two receivers were used, one in Czech Republic and one in France. The great circle paths of signal are shown in Fig. 4. This configure was chosen to study earthquake precursors in the Mediterranean region, which is seismically active due to the northward convergence (4-10 mm/yr) of the African plate with respect to the Eurasian plate along a complex plate boundary.

Very simple experimental setup was used to obtain field strengths. Loop antenna made of twenty turns of enameled wire was connected to the JFET preamplifier and NE5534 precision instrumental amplifier. Amplified signal was fed to the sound card of an ordinary personal computer with a sampling frequency of 196 kHz. Sampling frequency of sound card is according to Shanon-Kotelnikovov theorem sufficient for

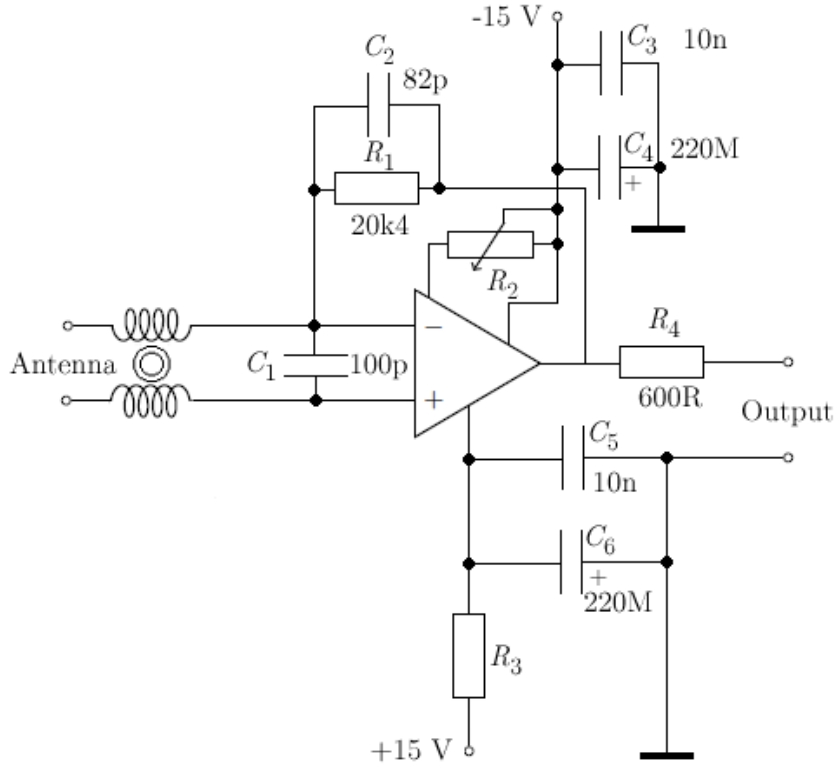


Figure 5: Schematics of VLF amplifier

VLF signals. 2^{16} -bin fast Fourier transformation was performed with custom software by Cooley–Tukey algorithm to obtain the frequencies of interest. This experimental apparatus was precisely calibrated with the procedure described in Jean et al. (1961), using an electromagnetic filed form one-loop coil placed in known distance from the receiver coil. Only change in this calibration procedure was the replacement of a precise thermal milliamperemeter with a non-inductive shunt resistor and digital oscilloscope to obtain the RMS values of the current flow to the calibration coil.

The amplifier is designed very simply. Schematic diagram of the amplifier is shown in Figure 5. This amplifier has high impedance input designed for direct connection to loop antenna. The input signal is limited by the input diode limiter of the fast diodes. Then it is fed to the operation amplifier, which also works as a bandpass filter (its parameters depend on R_1 and C_2). Ratio of resistances of R_1 and R_2 determines the gain of the amplifier.

Basic characteristics of loop antenna

The coil antenna is formed by an air coil, so it is sensitive to the magnetic component of electromagnetic waves, unlike conventional antennas. Faraday law of induction states that the electromotive force $e(t)$ is directly proportional to the time change of the magnetic flux Φ :

$$e(t) = -\frac{d\Phi(t)}{dt} \quad (2)$$

This relation is only valid for the antenna which are "electrically short" relative to the wavelength of the received electromagnetic waves, which is true for the VLF waves.

For the magnetic flux we can write

$$\Phi = \mathbf{B}(t) \cdot \mathbf{S}, \quad (3)$$

where $\mathbf{B}(t)$ is the vector of magnetic induction and \mathbf{S} normal vector of the loop plane. For the magnetic component of sinusoidal electromagnetic waves we can write

$$\mathbf{B}(t) = \mathbf{B}_0 \cos(\omega t).$$

Substituting this into eq. (3) we obtain for magnetic flux

$$\Phi(t) = \mathbf{B}_0 \cos(\omega t) S \cos \theta,$$

where θ is angle between vectors \mathbf{B}_0 and \mathbf{S} . If we assume number N of loops, equation (2) can be written as

$$e(t) = N A \mathbf{B}_0 \omega \sin(\omega t) S \cos \theta,$$

where A is the area of one loop. Because $\omega = 2\pi f$, effective value of electromotive force will be

$$U_{RMS} = 2\pi N A f B_{RMS} \cos \theta. \quad (4)$$

The dependence of the induced voltage on the electrical intensity

Antenna efficiency is determined by the so-called effective height of h_e , while this equation holds:

$$U_{RMS} = h_e E_{RMS}.$$

Here h_e is effective height in meters a E_{RMS} the effective value of the electric field strength in $V \cdot m^{-1}$.

If we consider that $c = \lambda f$ and the electric field intensity is bound to magnetic induction by the speed of light, thus the $E = cB$, we finally obtain by application of equation (4) for effective antenna height

$$h_e = \frac{2\pi N A \cos\theta}{\lambda} \quad (5)$$

From the equation(5) we can see that for VLF wavelengths (15 km for the frequency 20 kHz) the effective height of the loop antenna is very small compared to the signal wavelength. However, even with the loop antenna, it is possible to achieve good results.

The dependence of the induced voltage on the magnetic induction

The magnetic field around the coil depends on the magnetic component of electromagnetic wave, described by the intensity of magnetic field H and permeability coil of the core. We can write

$$\mathbf{B} = \mu_0 \mu_r \mathbf{H},$$

where μ_0 is the permeability of vacuum ($\mu_0 = 4\pi \cdot 10^{-7} \text{ H}\cdot\text{m}^{-1}$) and μ_r relative permeability of the core material. For air coil $\mu_r = 1$.

For the effective value of the voltage at the antenna assembly then this equation holds:

$$U_{RMS} = 2\pi \mu_0 \mu_r N A f H_{RMS} \cos\theta. \quad (6)$$

Equivalent circuit for loop antenna

Equivalent circuit for loop antenna is in Fig. 6. It consists of an ideal voltage source with a voltage according to the equation (6), radiation resistance R_{rad} , loop inductance L_c , wire inductance L_D , wire resistance R_D , resistance due to skin effect R_{AC} a the capacity of the loop coil capacitance C_C .

Radiation resistance describes the loss in the conversion of electromagnetic energy into electrical energy. Unlike the ohmic resistance, radiation resistance does not generate thermal noise by Johnson-Nyquist law. For value of the radiation resistance we can write

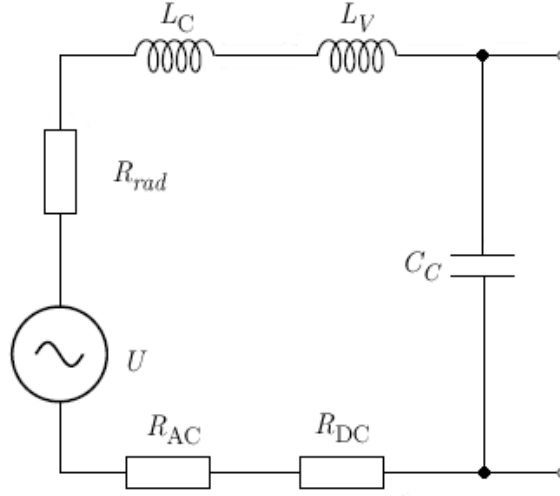


Figure 6: Equivalent electric circuit of loop antenna

$$R_{rad} = \frac{2}{3}\pi Z_0 \left(\frac{h_e}{\lambda} \right)^2 = \frac{8}{3}\pi^3 Z_0 \left(\frac{N\mu_0 A}{\lambda^2} \right)^2,$$

where Z_0 is impedance of free space (ca. 337Ω).

Loop inductance L_C : in the case inductance of rectangular coil wound on the frame with an edge length a equals

$$L_c = 8 \cdot 10^{-7} a N^2 \left(\ln \frac{1.4142 a N}{(N+1)l} + \frac{(N+1)l}{3aN} + 0.37942 \right),$$

where l is width of the winding (length perpendicular to the area of rectangle).

Wire inductance L_V is caused by the wire winding and its size approximately

$$L_V = \frac{\mu_0 4aN}{2\pi} \left(\frac{d}{8aN} - 1 - \frac{\mu_r}{4} + 2.303 \log \frac{16aN}{d} \right)$$

DC resistivity of wire R_{DC} is the function of length and diameter of the used wire. For the length of $4aN$ its values is

$$R_{DC} = \frac{4aN\rho}{\frac{\pi d^2}{4}},$$

where ρ is the resistivity wire, in the case of copper $\rho_{Cu} = 16.78 \text{ n}\Omega \cdot \text{m}^{-1}$. This resistance is a source of thermal noise by Johnson-Nyquist formula expressing the spectral density of thermal noise voltage as

$$\nu_{noise} = \sqrt{4kTR_{DC}} \left[\frac{\text{V}}{\text{Hz}^{1/2}} \right],$$

where k is Boltzmann constant a T thermodynamic temperature.

Resistance due to skin effect R_{AC} is the result of an inhomogeneous distribution of high-frequency current in the conductor. The current density near the surface is greater than near its center. For the size of the AC resistance caused by the skin effect caused by alternating current with frequency f we can write

$$R_{AC} = \frac{4aN}{\pi d} \sqrt{\pi\mu_0 f \rho}.$$

Loop coil capacitance C_C for an air loop winding of length l is approximately

$$C_C = 3.9685 \cdot 10^{-13} \sqrt{\frac{(400a)^4}{\pi}} \frac{1}{100l} [\text{F}].$$

for the ionospheric observations antenna with side length $a = 40$ cm and 50 loops of enameled copper wire with diameter 0.4 mm^2 was designed.

3.2 Data analysis

Data were analysed using Pearson's coefficient. Pearson product-moment correlation coefficient is according to Kendall and Stuart (1973) the covariance of the two variables divided by the product of their standard deviations (see chapter 1.5). The form of the definition involves a "product moment", that is, the mean (the first moment about the origin) of the product of the mean-adjusted random variables; hence the modifier *product-moment* in the name.

Pearson's coefficient (sometimes referred to as the PPMCC or PCC or Pearson's r) is a measure of the linear correlation between two variables X and Y , giving a value between $+1$ and -1 inclusive, where 1 is total positive correlation, 0 is no correlation, and -1 is total negative correlation.

Data were investigated by calculating Pearson product-moment correlation coefficient for table with ACF minimum positions in one row and 1 or 0 (earthquake or no earthquake) in the second. For all earthquakes in selected region no direct correlation was found, but for earthquakes with preparation zones under VLF propagation path the Pearson correlation coefficient was calculated as 0.954 . Using table of critical values for two-tailed test from Freund (1984), the significance level is better than $\alpha=0.02$.

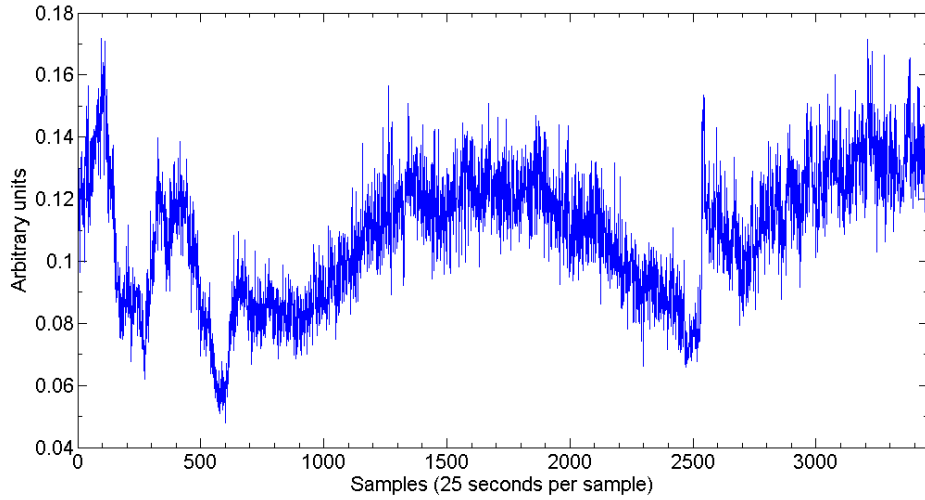


Figure 7: Typical 24-hour data – VLF signal amplitude

4 Results

Typical data series (captured twenty-four hour record) acquired with the described experimental set-up is in Fig. 7. Reflectivity of the ionosphere for VLF radio waves varies on several time scales. The most significant is the diurnal variation with a maximum at noon, which follows the dependence of the ionosphere irradiation:

$$I = \frac{E}{r^2} \cos \Psi,$$

where E is solar irradiance, r distance between Sun and Earth and Ψ is the angle of incidence of solar rays. Significant signal drops during sunrise and sunset are caused by destructive interference of waves reflected from the ionosphere and terrestrial waves.

One can clearly see that signal is scintillating – this is a consequence of the existence of random electron-density fluctuations within the ionosphere.

Obtained time series of scintillating signal was treated with following matlab script:

```
load data.txt
x=data(:,3)
X=x-smooth(x,120);
C=xcorr(X,X);
c=C(8640:end);
c=c(1:600);
plot(c);
[B,I] = min(c);
text(500,500,strcat('Minimum ', num2str(B,3), ' in ',
    num2str(I)), 'HorizontalAlignment', 'center');
```

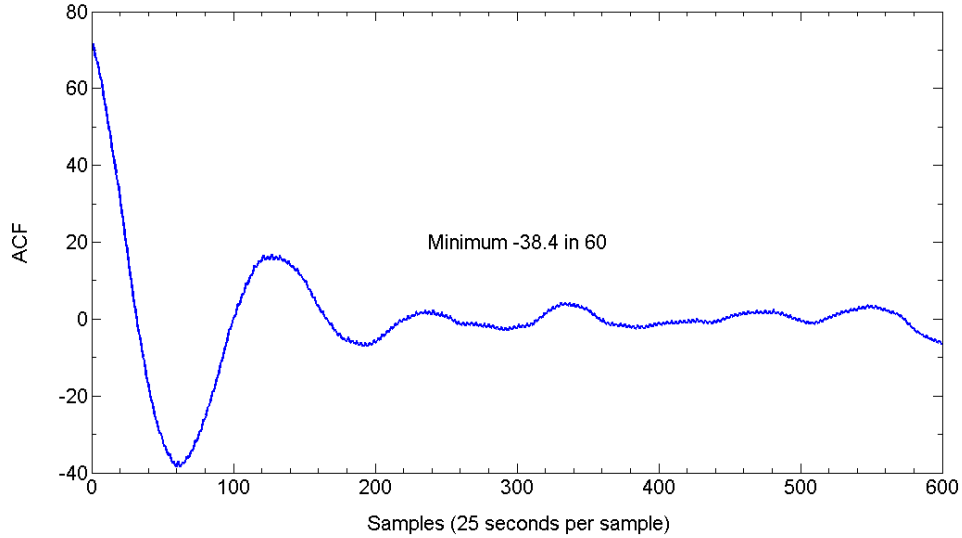


Figure 8: Autocorrelation of the 24-hour VLF data

Data are loaded from the text file, the diurnal variation is subtracted and the autocorrelation is calculated as cross-correlation of the data set with itself. Only the first 600 samples are plotted and the position of the first minimum and its value is calculated and added to graph. Typical results are in Fig. 8. Graph indeed shows zeroth-order Bessel function of the first kind.

Signals from several VLF transmitters were studied over the whole year and it seems that the parameters of this Bessel function depends a) on the frequency of transmitter and b) on the time of year (see Fig. 8).

The integral representation of Bessel function of the first kind and zeroth order is according to Stuber (1996)

$$J_0(x) = \frac{1}{2\pi} \int_{-\pi}^{\pi} e^{ix \sin t} dt.$$

If we assume signal strength at the antenna as result of the superposition of (for simplicity) two plane waves of the same frequency, the other reflected from the ionosphere so that the two copies have angular separation θ . Then their correlation would vary like $e^{ix \cos \theta}$, because the the projection of the wavelength of the other wave along the direction of propagation of the other gets multiplied by $\cos \theta$. Now we can treat θ as a random variable uniformly distributed over the circle and compute the average. Thus the Bessel function emerges as a consequence of the underlying geometry.

Ionosphere is very dynamic medium and the ionospheric scintillation emerges as result of continual electron density fluctuation ΔN . Signal scattering in random me-

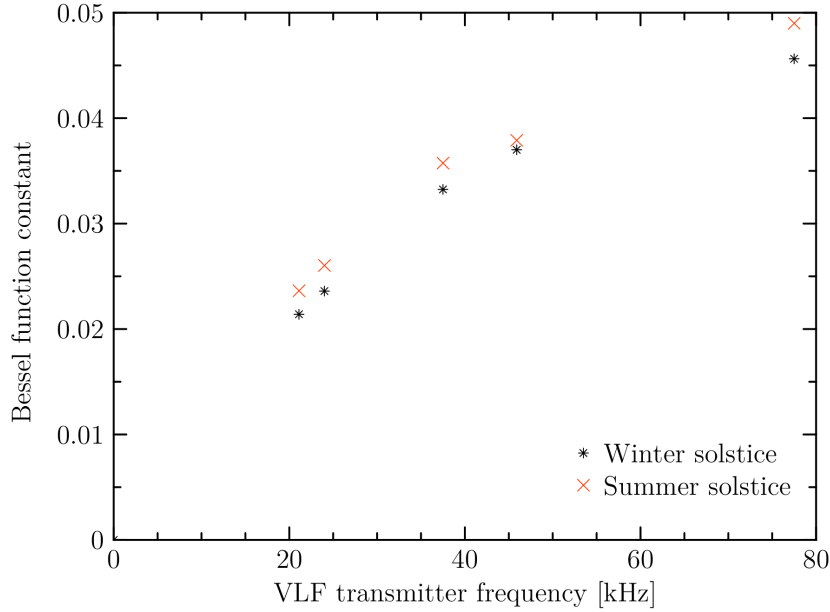


Figure 9: Bessel function constant for different transmitter frequencies during the year

dia was studied extensively and stochastic properties of signals propagation through random irregular electron density structures is treated extensively by Kung (1982).

If we assume that an irregularity slab can be characterized by a dielectric permittivity

$$\epsilon = \langle \epsilon_1 \rangle [1 + \epsilon_1(\mathbf{r}, t)],$$

where $\langle \epsilon_1 \rangle$ is the background average dielectric permittivity which for ionosphere is given by

$$\langle \epsilon_1 \rangle = (1 - f_{p0}^2/f^2)\epsilon_0$$

and $\epsilon_1(\mathbf{r}, t)$ is the fluctuating part characterizing the random variations caused by the irregularities and is given by

$$\epsilon_1(\mathbf{r}, t) = \frac{(f_{p0}/f)^2[\Delta N(\mathbf{r}, t)/N_0]}{1 - f_{p0}^2/f^2}.$$

Here, f_{p0} is the plasma frequency corresponding to the background electron density N_0 and f is the frequency of the incident wave. In the percentage fluctuation $\Delta N/N_0 = 5$, the temporal variations, caused by either the motion of irregularities as in a frozen flow or the turbulence evolution as in a nonfrozen flow, or both, are assumed to be much slower than the period of the incident wave.

As the wave propagates through the irregularity slab, to the first order, only the phase is affected by the random fluctuations in refractive index. This phase deviation

is equal to $k_0(\Delta\phi)$, where k_0 is the free space wave-number and $\Delta\phi$ is the optical path fluctuation:

$$\Delta\phi(\boldsymbol{\rho}) = -\frac{e^2}{2m\epsilon_0\omega^2}\Delta N_T(\boldsymbol{\rho}) = -\frac{\lambda^2}{2\pi}r_e\Delta N_T(\boldsymbol{\rho}),$$

where e is the electronic charge, m is its mass, ω is the circular radio frequency, r_e is the classical electron radius and $\boldsymbol{\rho} = (x, y)$ is the transverse coordinate. The deviation in the total electron content defined by

$$\Delta N_T(\boldsymbol{\rho}) = \int \Delta N(\boldsymbol{\rho}, z)dz.$$

Therefore, after the wave has emerged from the random slab, its phase front is randomly modulated. As this wave propagates to the ground, the distorted wave front will set up an interference pattern resulting in amplitude fluctuations.

It should be noted that other phenomena also plays role in scattering process: According to Stuber (1996) and with after-mentioned assumption of uniform distribution of θ over $[-\pi, \pi]$ we can write for the auto-correlation function

$$ACF = \frac{1}{2\pi} \int_{-\pi}^{\pi} \cos(2\pi f_d t \cos \theta) d\theta = J_0(2\pi f_d t),$$

where $J_0(x)$ is the modified Bessel function of the first kind and is zero-order. In the case of VLF waves scattered by ionosphere, there is no Doppler shift caused by motion of the transmitter or receiver, but there are small effects due to radial motion of the plasma (Saxton, 1989), which are of order of 0.1 Hz. Nonlinear electron cyclotron resonance interaction near equator can also cause substantial changes in frequency and phase of the received signal (Clilverd et al., 2001). The position of the first minimum of the Bessel function then should be proportional to the constant $2\pi f_d$.

The penetration of electric field of seismic source into the plasmasphere causes formation of a VLF duct. Inside this duct cyclotron-resonance interaction between waves and particles leads to precipitation of energetic electrons into the lower atmosphere, finally leading to the increase in electron density in the ionospheric D-region (details of this mechanism can be found in Pulinetz (2004)). It was proposed that the additional electric field in the ionosphere cause the electric currents and turbulence. Hegai et al. (1997) calculated that for sufficiently strong electric field of short duration very anisotropic disturbances emerges with much longer duration than primary pulse of the electric field.

For the work described in this thesis this question is crucial: Why the auto-correlation function changes during the course of year? For consecutive days the constant $2\pi f_d$ remains almost the same, but it changes slowly during the year. If the assumption of the radial motion of plasma is correct, in summer with higher temperatures and more energy from Sun the motion will be more apparent, as well as the ionisation of the ionosphere. According to Pulinets and Boyarchuk (2004, pg. 162), cyclotron resonance interaction between waves and particles inside the VLF duct in the radiation belt region is consequence of penetration of the electric field of seismic source into the plasmasphere and the cause of the increase of electron density in the ionospheric D-region, finally leading to the increase in electron density in the ionospheric D-region. Anisotropic disturbances caused by electric currents and turbulence described in part 1.3 may also play an important role. If this assumption is correct, the properties of auto-correlation function can be used as earthquake precursor.

Over forty earthquakes with magnitude $M \geq 4.5$ were studied over the course of year, best results were obtained for M5.0+ earthquakes. In the Fig. 10 are typical results. For M4.6 earthquake near Sami, Greece on 4 March 2015 at 04:38:20 UTC the ACF have evident deviation the day prior the earthquake (Fig. 10a). This earthquake with preparation zone of radius ~ 95 km (marked 1 in fig. 4) was apparent in data received in France, not in the Czech Republic.

Fig. 10b shows the ACF values for M5.6 earthquake near Adamas, Greece on 29 July 2015 at 03:45:06 UTC. This earthquake with preparation zone of radius ~ 310 km (marked 2 in fig. 4) was apparent in data received both in France and Czech Republic. The average value of ACF is higher than for the Sami earthquake. That is caused by fact that this earthquake was in summer. Despite the fact that this earthquake had greater magnitude, the deviation is not as prominent as in the case of the Sami earthquake. This effect was present in all the data and there is strong link between the depth of the epicenter and deviation in auto-correlation function (the Sami earthquake had epicenter in depth of 11 km, the Adamas in 80 km).

For earthquakes with preparation zones far from the great circle paths of VLF signals no changes were observed (for example M4.5 earthquake near Palaikastron on 17 April 2015 at 16:39:42 UTC with epicentre depth of 27.8 km, marked 3 in fig. 4). It seems that the radius ρ of the earthquake preparation zone calculated according to

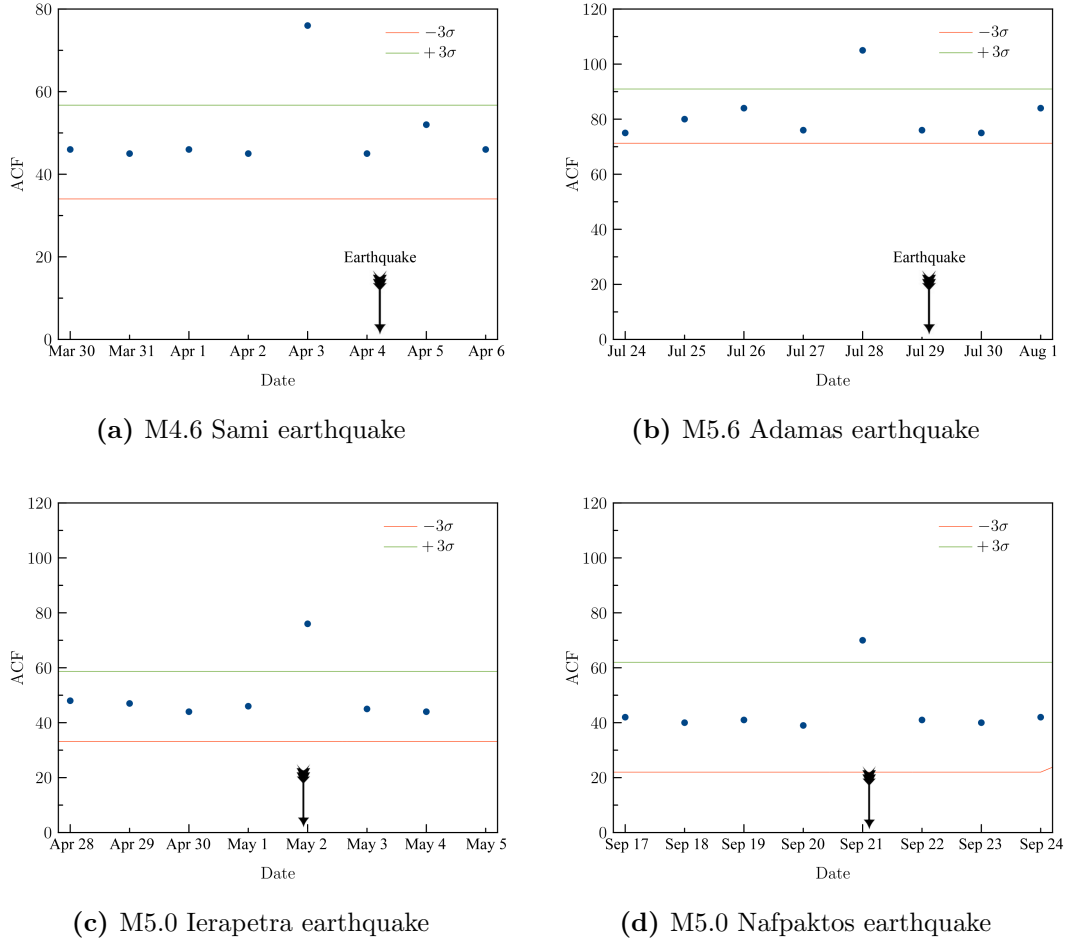


Figure 10: Typical behaviour of ACF prior $M \geq 4.5$ earthquakes

Dobrovolsky et al. (1979) as

$$\rho = 10^{0.43M} \text{ km}, \quad (7)$$

where M is the magnitude, is a good clue to the estimation if the earthquake can be predicted with this method.

Data were statistically investigated by calculating Pearson product-moment correlation coefficient for table with ACF minimum positions in one row and 1 or 0 (earthquake or no earthquake) in the second. For all earthquakes in selected region no direct correlation was found, but for earthquakes with preparation zones under VLF propagation path the Pearson correlation coefficient was calculated as 0.954. Using table of critical values for two-tailed test from Freund (1984), the significance level is better than $\alpha=0.02$.

This result is not surprising, theoretical calculations (Pulinets et al. 1998) show that the vertical ground electric field starts to penetrate effectively into the ionosphere

and create irregularities of electron concentration when the size of the area on the ground surface occupied by the anomalous field exceeds 200 km in diameter. This area could be identified with the zone of earthquake preparation (Dobrovolsky et al. 1979) or by another determination the precursory seismic activation zone (Bowman et al. 1998). Here the usual precursors used in seismology are borne in mind, fore-shocks, deformations, seismic waves velocity anomalies, etc. Using the Dobrovolsky formula for $\rho = 100$ km we obtain $M=4.65$. In the paper of Garavaglia et al. (2000) a good correlation between observed deformations and radon emanations is reported, so we can identify the size of the earthquake preparation zone used in seismology with scale parameter used for the zone occupied by the anomalous electric field. The changes in radon concentration are due to the deformations and crack formation in the Earth's crust, so they should be observed within the zone of earthquake preparation. Using the estimate above we can expect the ionosphere reaction from earthquakes with a magnitude higher than 4.65. Another factor for estimation is simple scaling. The first most conducting layer of the ionosphere, the E-layer, is at the altitude ~ 100 km, and the electric field starts to penetrate into the ionosphere when its spatial scale reaches the size of the height of the ionospheric layer. We can say that a quantity between 100 and 200 km is a transition size for the electric field's area and the correspondent ionosphere reaction, which is shown by the results of statistical studies (Chen et al. 1999).

It should be also noted that method described in this work is useful only for shallow earthquakes e.g., for earthquakes with epicentres in depth up to about 40 km, as can be seen from Table 1.

Because the used method is similar to the observational techniques described in Hayakawa (2015), data were examined to also study the terminator effect. Normal terminator effect is associated with phase changes of received components of diffracted waves during sunrise and sunset, manifested by minima in received VLF signal diurnal variation (both for the amplitude and phase). "Anomalous" terminator effect, described for example in Yoshida et al. (2008), is shift in this terminator times (in which the received wave amplitude or phase is minimal) the day or days prior the earthquake. This effect was observed for M6.0+ earthquakes and is not present in data from TBB transmitter studied in this work. This was tested by calculating ACF minimum position for 10-minute samples during the day and checking their behaviour for days before

Date	Depth	Magnitude	Place	ACF change
24.7.2015	141	5.1	14km WSW of Kefalos, Greece	no
20.6.2015	15	5.0	84km SSE of Makry Gialos, Greece	yes
9.6.2015	16	5.4	52km ESE of Palaikastron, Greece	yes
9.6.2015	13	5.3	11km ENE of Larimna, Greece	yes
2.5.2015	13	5	62km S of Ierapetra, Greece	yes
17.4.2015	15	5.3	52km ESE of Palaikastron, Greece	yes
16.4.2015	10	5.0	57km SSW of Karpathos, Greece	yes
16.4.2015	20	6.0	49km SW of Karpathos, Greece	yes
27.3.2015	67	5.2	58km WNW of Karpathos, Greece	no
28.1.2015	37	5.1	60km S of Pargos, Greece	no
29.12.2014	7	5.0	25km S of Ulcinj, Montenegro	yes
6.12.2014	12	5.1	12km SW of Plomarion, Greece	yes
22.11.2014	32	5.6	5km E of Panciu, Romania	no
17.11.2014	10	5.1	9km NE of Malesina, Greece	yes
17.11.2014	23	5.4	11km SSE of Limni, Greece	yes
8.11.2014	18	5.1	9km SSW of Argostolion, Greece	yes
7.11.2014	18	5.1	9km SSW of Argostolion, Greece	yes
24.10.2014	0	5.3	6km SW of Krikellos, Greece	yes
3.10.2014	15	5.1	74km SSE of Makry Gialos, Greece	yes
21.9.2014	11	5.0	4km S of Nafpaktos, Greece	yes

Table 1: M5.0+ earthquakes studied in this work with epicentre depth.

and after the earthquake. It was found that these values are well correlated (average Pearson's correlation coefficient is around 0.7 for consecutive days) and no significant changes were found for days prior the earthquake. It was noted that these samples had higher values the day before earthquake, which is not surprising, because the overall value calculated from the whole 24-hour data for day immediately before the earthquake have higher value of ACF minima position that for the other days. What is interesting is the fact that the values during the time when the Sun is above the horizon show nearly the same values of ACF minima position and the main difference (higher values) occurs at night. This is caused by the behaviour of the ionosphere at night, when its ionization is not affected by radiation from the Sun.

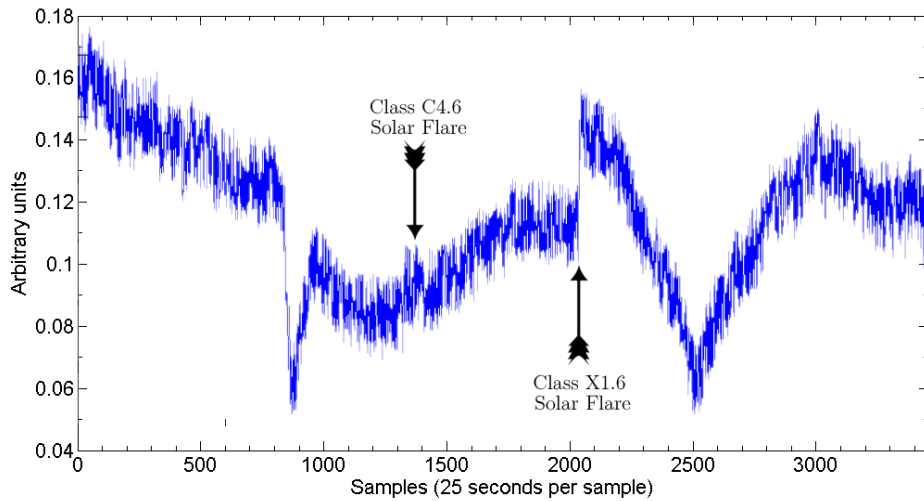


Figure 11: 24-hour VLF data with solar flares

4.1 Other dynamic phenomena that could influence ACF

As it was previously stated, ionosphere is very dynamic medium. Other physical phenomena not related to earthquakes can change the properties governing the scattering of VLF waves. Impact of these processes must be ruled out. Two main influences have been taken into account:

4.1.1 Solar flares

It is well known that ionization of the lower ionosphere can increase considerably during chromospheric flares on the Sun as the X-ray and UV part of the solar spectrum penetrates the D-layer and the VLF wave strength during such a flare can either increase or decrease due to changes in the geometry of propagation. These density variations are different for different altitudes and are called Sudden Ionospheric Disturbances, SIDs. Details can be found for example in (Mitra 1974) or (Davies 1990).

Figure 11 shows day with two solar eruption – class C4.6 and class X1.6 ¹. Even for this solar flare of October 22 no significant change in 24-hour ACF data was found (see Fig. 12).

Extensive statistical study of significant solar flares (up to this X1.6 level, influ-

¹Solar flares are classified as A, B, C, M or X according to the peak flux (in watts per square metre) of 100 to 800 picometre X-rays near Earth, as measured on the GOES spacecraft. Class letter denotes magnitude of flare – C is 10^{-6} , X 10^{-4} . Within a class there is a linear scale from 1 to 9, so an X2 flare is twice as powerful as an X1 flare, and is four times more powerful than an M5 flare.

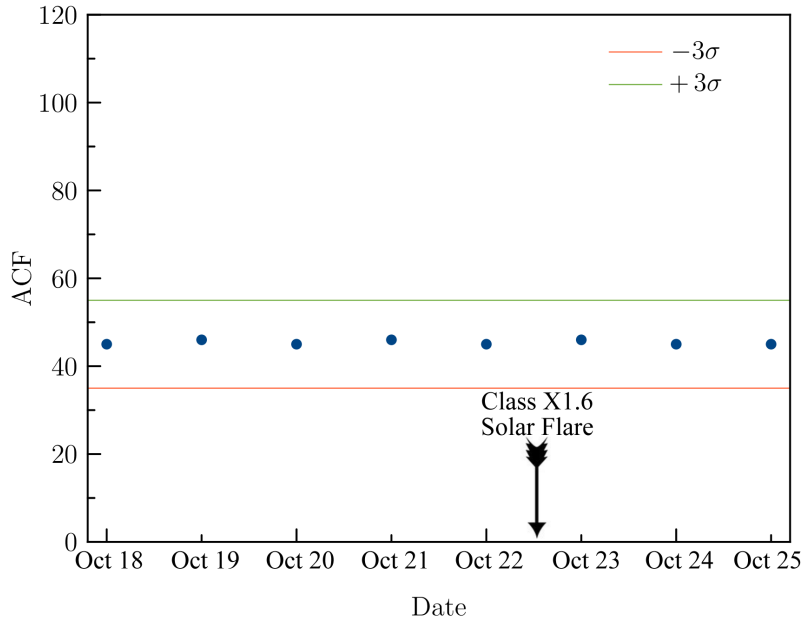


Figure 12: Behaviour of ACF minimum position prior and after solar flare

encing the TBB transmitter signals during the survey period) showed that these flares had statistically negligible ($\alpha=0.05$) influence on ACF function computed over 24-hour period.

4.1.2 Magnetic storms

This topic is treated extensively for example by Chakraborty et al. (2015). The main source of the magnetic storms is severe irregularities in the solar wind. Regardless of their origins (solar mass ejections, proton events, solar flares, etc.) their final product in the vicinity of the Earth’s magnetosphere is strong changes in the interplanetary magnetic field interacting with the magnetosphere. According to Gonzalez et al. (1994) ”the geomagnetic storm is an interval of time when a sufficiently intense and long lasting inter planetary convection electric field leads, through a substantial energization in the magnetosphere -ionosphere system, to an intensified ring current sufficiently strong to exceed some key threshold of the quantifying storm time D_{st} index”. This index is a quantitative measure of the ring current forming around the Earth during the geomagnetic storm and supported by the ions with energies of several tens of keV and electrons with energy near 10 keV. It is commonly accepted that the magnetic storm is triggered by the large dawn-to-dusk electric field produced by the southward turn of

the interplanetary magnetic field B_z .

The electric field leads to the earthward plasma convection, which permits high-energy particles to flow into near-earth space (Ondoh and Marubashi 2001). The ring current, and other currents of modified magnetospheric convection during the magnetic storm induce the variations of magnetic field on the ground surface that could be measured by magnetometers. The network of the reference magnetometers equally distributed along longitude within the latitudinal band $21 - -33^\circ$ give the quantitative contribution to calculate the D_{st} index. It is commonly agreed that the magnetic storm can develop when the D_{st} index exceeds the threshold -50 nT (which corresponds to the interplanetary B component -5 nT) and stay over this threshold at least 2 hours (Gonzalez et al. 1994). There are other indices to describe the geomagnetic activity (K_p , A_p , a_p , etc.) but all of them have a contribution from the high latitude activity and can show the increase without development of the magnetic storm, so called substorms, which are out of the scope of this work and can be found in Dieminger et al. (1996).

The ionospheric effects of the magnetic storm is a very complex phenomenon of increased dissipation of the solar wind energy, probably one of the most complex in ionospheric physics involving a lot of changes in the ion composition, substantial changes in plasma temperature and concentration, etc. Practically all ionospheric parameters are affected by the magnetic storm. The attempt to describe the global picture of the ionospheric storm effects using the data provided by a ground based ionospheric station network is made in the work by Szuszczewicz et al. (1998), and using the top-side sounding data from the Intercosmos-19 satellite is described in Karpachev et al. (1995). The empirical model of the magnetic storm now included in the IRI describing the variations of the ionosphere parameters during the storm is published in the work by Araujo-Pradere (2002), and effects of the magnetic storm in all regions of the ionosphere and thermosphere – in Danilov and Lastovicka (2002).

Intense geomagnetic storms caused by coronal mass ejections (CMEs) can alter ionospheric scintillation and total electron contents (TEC) which is defined as

$$TEC = \int_S^R n_e(l)dl,$$

where $n_e(l)$ is the electron density along the signal path from source (S) to receiver (R). These effects are apparent near the magnetic equator where the equatorial vertical plasma drift takes place. During magnetic storms strong eastward (westward) electric field from the magnetosphere (disturbance dynamo) can penetrate to equatorial region

intensifying (or weakening) the upward plasma drift and consequently triggering (or inhibiting) the ionospheric irregularities. For details see for example (Fejer, 1999). As can be deduced from Atulkar et al. (2014), these effects are much less pronounced at higher latitudes so the influence of moderate magnetic storms on the ACF are negligible. Only very strong geomagnetic storms could impact electron density at high latitudes (Truhlik et al., 2011).

During the magnetic storm main phase, relativistic electrons (with energies higher than 1 MeV) can precipitate from the plasma-pause to ionosphere, altering its conductivity due to changes in electron density (details can be found for example in Thorne and Kennel (1971)). These changes can affect the received VLF signal amplitude. According to Demirkol et al. (1999) the VLF response is largely due to 100 – 300 keV electrons that accompany the 2 – 5 MeV electrons that signify relativistic electron enhancement events, because these are the particles which produce most of the ionization enhancement in the D-region where the VLF waves reflect.

This ionospheric effects are observed only when the electron flux is above 3×10^3 electrons/cm² · sr · s, apparently because of the fact that the VLF signature of the enhancement for lower fluxes is suppressed by other ionospheric variations.

These effect have to be taken into account for strong geomagnetic storms, but these events evolve on the longer time scales than are the oscillations of the VLF signal amplitude.

Conclusion

The correlation between the position of the first minimum of ACF and seismic activity in earthquake preparation zone was proven on uncertainty level better than 3σ . This deviation is higher for the shallow earthquakes. Theoretical explanation of the phenomenon is proposed taking into account the penetration of the anomalous electric field into the ionosphere leading to increased ionization of the D-region.

This effect can be caused by the penetration of electric field of seismic source into the plasmasphere and formation of a VLF duct. Inside this duct cyclotron-resonance interaction between waves and particles leads to precipitation of energetic electrons into the lower atmosphere, finally leading to the increase in electron density in the ionospheric D-region. Also the dynamics of the plasma motion can change, leading to ACF changes too.

The method of earthquake prediction relies on the calculation of the position of autocorrelation function first minimum, describing the stochastic properties of the reflected VLF waves (position of this first minimum is inversely proportional to the frequency of Bessel function of the autocorrelation function). Changes in this minimum position have direct correlation to the earthquake in the next 24 hours in the area directly below the great circle path of the VLF waves.

This method has the same advantages as other VLF techniques described in Haya-kawa (2015) – simple equipment and data processing. It was showed that for shallow earthquakes the threshold magnitude is around 4.5 for earthquakes with preparation zone under the great circle path of VLF signal and best results are for earthquakes with magnitudes greater than 5. The main disadvantage is that this method cannot be used to predict earthquakes with deeper epicentres.

Annex A presents original paper published by the author in Journal of Seismology summarising results of this thesis.

References

- Araujo-Pradere, E. A., Fuller-Rowell, T. J., Codrescu, M. V.: STORM: An empirical stormtime ionospheric correction model – 1. model description. *Radio Sci.* 37: Art. No 1070.
- Atulkar, R., Bhardwaj, S., Khatarkar, P., Bhawre, P., Purohit, P. K.: Geomagnetic Disturbances and Its Impact on Ionospheric Critical Frequency (foF2) at High, Mid and Low Latitude Region, *American Journal of Astronomy and Astrophysics*. Vol. 2, No. 6, 2014, pp. 61-65. doi: 10.11648/j.ajaa.20140206.11
- Bak, P., Tang, C., Wiesenfeld, K.: Self-organised criticality. *Phys Rev A*, 38, 1988. pp. 364.
- Blaunstein, N., Plohotniuc E.: *Ionosphere and Applied Aspects of Radio Communication and Radar*. CRC Press 2008. Print ISBN: 978-1-4200-5514-6
- Boyarchuk, K. and Pulinets, S.: *Ionospheric Precursors of Earthquakes*. Springer-Verlag Berlin Heidelberg, 2005.
- Bowman, G.G. and Hajkowitz, L. A.: Small-scale ionospheric structures associated with mid latitude spread-F. *J. Atmos. Terr. Phys.*, Vol. 53, 1991, pp. 4447-4457.
- Bowman, D. D., Ouillon, G., Sammis, C. G., Sornette, D.: An observation test of the critical earthquake concept. *J. Geophys. Res.*, 103, 1998. pp. 22,359-24,372.
- Bracewell, R.: *The Autocorrelation Function. The Fourier Transform and Its Applications*. New York: McGraw-Hill, pp. 40-45, 1965.
- Chakraborty M., Kumar S., Barin K. D., Guha, A.,. Effects of geomagnetic storm on low latitude ionospheric total electron content: A case study from Indian sector. *Journal of Earth System Science*. July 2015, Volume 124, Issue 5, pp 1115-1126
- Chen, Y. I., Chuo, J. Y., Liu, J. Y., Pulinets, S. A.: Statistical study of ionospheric precursors of strong earthquakes at Taiwan area. XXVI URSI General Assembly, Tronot, 1999. Abstracts, p. 475.
- Clilverd, M. A., C. J. Rodger, N. R. Thomson, and K. H. Yearby (2001), Investigating the possible association between thunderclouds and plasmaspheric ducts, *J. Geophys. Res.*, **106(A12)**, 29771-29781
- Danilov, A. D., Lastovicka, J.: Effects of geomagnetic storms on ionosphere as the possible precursor of Tashkent earthquake. *Dokl. Uzbek. Acad. Sci.* No 12: 30-32.
- Davies K., 1990. *Ionospheric radio*, Peter Peregrinus, London, 580 pp.
- Dieminger W., Hartmann, G. R., Leitinger R. (eds): *The upper atmosphere. Data analysis and interpretation*. Springer-Verlag.
- Demirkol, M. K., Inan, U. S. Bell, T. F., Kanekal, S. G. and Wilkinson, D. C. Ionospheric effects of relativistic electron enhancement events. *Geophysical Research Letters*. 26(23), 3557–3560, doi:10.1029/1999GL010686.

- Dobrovolsky, I. R., S. I. Zubkov, and V. I. Myachkin, 1979: Estimation of the size of earthquake preparation zones. *Pageoph.*, **117**, 1025-1044.
- Fejer, B., Cherlies, L. S., DePaula, E. R.: Effects of the vertical plasma drift velocity on the generation and evolution of equatorial spread F, *J. Geophys. Res.*, 104 (A9), 19859-19869.
- Fremouw, E.J., Secan, J.A.: Modelling and scientific application of scintillation results, *Radio Sci.* 19, 1984, pp. 687-694.
- Freund, J. Modern elementary statistics. Englewood Cliffs, N.J: Prentice-Hall, 1984.
- Garavaglia, M., Dal Moro, G., Zadro, M.: Radon and tilt measurements in a seismic area: Temperature effects. *Phys. Chem. Earth*, 25, 2000. pp. 233-237
- Gokhberg, M. B., Gufeld, I. L., Marenko, V. F., Ponomarev, E. A., Rozohny, A. A., Yampolsky, V. S.: Studies of perturbations of natural and artificial electromagnetic fields by sources of seismic origin, *Izvestiya, Earth Physics* 23, 1987. pp. 102-108
- Gonzalez W. D., Joselyn, J. A., Kamide, Y. Kroehl, H. W., Rostoker, G., Tsurutami, B. T., Vasyliunas, V. M.: What is geomagnetic storm? *J. Geophys. Res*, 99, 1994. pp. 5771-5792
- Gufeld, I. L., Gusev, A. G., Pokhotelov, O. A.: Is the prediction of earthquake date possible by VLF radio wave monitoring method? In: Hyakawa M., Fujiniwa, Y. (eds.) *Electromagnetic phenomena related to earthquake prediction.* Terra Sci. Publ. 1994. pp. 381-390
- Hao, J., Tang, T., Li, D.: Progress in the research of atmospheric electric field anomaly as an index for short-impeding prediction of earthquakes. *J. Earthquake Pred. Res.* 8, 2000. pp. 241-255
- Hayakawa, M. (ed): NASDA's earthquake remote sensing for niter research. Seismo-electromagnetic phenomena in the lithosphere, atmosphere and ionosphere. Final report. The university of electro-communications, Chofu, Tokyo, Japan 2001.
- Hayakawa M., Raulin J. R., Kasahara Y., Bertoni F. C. P., Hobara Y. and Guevara-Day W.: Ionospheric perturbations in possible association with the 2010 Haiti earthquake as based on medium-distance sub ionospheric VLF propagation data. *Nat Hazard Earth Syst Sci*, 11 (2011) 513.
- Hayakawa M.: *Earthquake Prediction with Radio Techniques.* John Wiley & Sons 2015. doi: 10.1002/9781118770368.ch1
- Hegai, V.V., Kim, V.P., and Nikiforova, L.I., A possible generation mechanism of acoustic-gravity waves in the ionosphere before strong earthquake, *J. Earthquake Predict. Res.*, 1997, no. 6, pp. 584-589.
- Heigi, V. V, Kim, V. P., Nikiforova, L. I.: A possible generation mechanism of acoustics gravity waves in the ionosphere before strong earthquakes. *J. Earthquake. Predict. Res.* 6, 1997. pp 584-589.

- Hewish, A.: The diffraction of radio waves in passing through a phase-changing ionosphere, *Proc. Roy. Soc. A.* 209, 1951, 81.
- Jean, A.G., Taggart, H.E., Wait, J.R., 1961. Calibration of loop antennas at VLF. *J. Res. Natl. Bur. Stand. Sect. C* **65** (July–September (3)).
- Kendall, M. G., Stuart, A. (1973) *The Advanced Theory of Statistics, Volume 2: Inference and Relationship*, Griffin. ISBN 0-85264-215-6 (Section 31.19)
- Karpachev, A. T., Deminova, G. F, Pulinets, S. A.: Ionospheric changes in response to IMF variations. *J. Atm. Terr. Phys.* 57, 1995. pp. 1415-1432
- Kim, V. P., S. A. Pulinets, and V. V. Hegai, 2002: Theoretical model of possible disturbances in the nighttime mid-latitude ionospheric D-region over an area of strong earthquake preparation. *Radiophys. Quantum Electronics*, **45**, 262-268.
- King C. Y.: Gas geochemistry applied to earthquake prediction: An Overview. *J Geophys Res*, 91 (1986) 12269.
- King J. W., Kohl, H.: Upper atmosphere winds and ionospheric drifts caused by neutral air pressure gradients. *Nature*, Vol. 206, 1965, pp. 899-701.
- Klusman, R. W.: Soil gas and related methods for natural resource exploration. Wiley, 1993. Chichester.
- Kossobokov, V. G., Keilis-Borok, V. I., Turcotte, D. L., Malamud, B. D.: Implications of statistical approach for earthquake hazard assessment and forecasting. *Pure Appl. Geophys.* 157, 2000. pp. 2323-2349.
- Kung Ch. Y., Chao-Han L., Radio wave scintillations in the ionosphere, in *Proceedings of the IEEE* , vol. 70, no.4, pp.324-360, April 1982 doi: 10.1109/PROC.1982.12313
- Knepp, D. L.: Multiple phase-screen calculation of the temporal behavior of stochastic waves, *Proc. IEEE* 71, 1983, pp. 722-737.
- Mitra A. P., 1974. Ionospheric effects of solar flares, D. Reidel, Norwell, Mass.
- Molchanov O. A., Hayakawa M., Oudoh T. and Kawai E.: Precursory effect in the sub-ionospheric VLF signals for the Kobe earthquake. *Phys Earth Planet Inter*, 105 (1998) 239.
- Perrone, L., Korsunova, L. P., and Mikhailov, A. V.: Ionospheric precursors for crustal earthquakes in Italy, *Ann. Geophys.*, 28, 941-950, doi:10.5194/angeo-28-941-2010.
- Plendl, H.: Concerning the influence of eleven-year solar activity period upon the propagation of waves in vireless technology. *Proc. Inst. Radio Eng.*, vol. 20, 1932. pp. 520-539.
- Pulinets, S., Boyarchuk, K.: *Ionospheric Precursors of Earthquakes*. Springer Verlag Publ 2004. ISBN: 978-3540208396
- Rappaport, T. S.: *Wireless communication*, IEEE Press, 1992.

- Ratcliffe, J. A.: Physics of the Upper Atmosphere. New York-London: Academic Press, 1960.
- Rees, M. H.: Auroral ionization and excitation by incident energetic electrons. *Planet. Space Sci.* 11, 1963. pp. 1209-1218
- Richmond, A. D.: Ionospheric Electrodynamics, pp. 249-290, In: Volland (Ed.), *Handbook of Atmospheric Electrodynamics*, Vol. II, Boca Raton: CRC Press, 1995.
- Rino, C.L.: On the application of phase screen models to the interpretation of ionospheric scintillation data, *Radio Sci.* 17, 1982, pp. 855-867.
- Rundle, J. B., Turcotte, D. L., Klein, W. (eds): *Geocomplexity and the Physics of Earthquakes*. Geophysical Monographs Series, American Geophysical Union, Washington D. C.
- Saxton, J. M., Smith, A. J.: Quiet time plasmaspheric electric fields and plasmasphere-ionosphere coupling fluxes at $L = 2.5$, *Planet Space Sci.*, **37**, 283-293, 1989.
- Shklyar, D. R., Nunn, D., Smith, A. J. and Sazhin, S. S.: An investigation into the nonlinear frequency shift in magnetospherically propagated VLF pulses, *J. Geophys. Res.*, 97(A12), 19389-19402
- Shlykar, D. R., Truhlik, V.: On the modification of light ion concentration profiles above seismically active regions: a qualitative consideration. *J. Atm. Solar Terr. Phys.* 60, 1998. pp. 1024-1033
- Scholz, C. H., L. R. Sykes, and Y. P. Aggarwal, 1973: Earthquake prediction: A physical basis. *Science*, **181**, 803-809.
- Spiegel, M. R.: *Theory and Problems of Probability and Statistics*, 2nd ed. New York: McGraw-Hill, p. 298, 1992.
- Stuber, G.L.: *Principles of Mobile Communication*. Boston: Kluwer Academic 1996. ISBN: 0792397320
- Szuszczewicz, E. P., Lester, M., Wilkinson, P., Blanchard, P., Abdu, M., Hanbaba, R., Igarashi, K., Pulinst, S, Reddy, B, M.: Global ionospheric storm characteristics during solar maximum equinox. *J. Geophys. Res.* 103, 1998. pp. 11,665-11,684
- Thorne, R. M., and C. F. Kennel (1971), Relativistic electron precipitation during magnetic storm main phase, *J. Geophys. Res.*, 76(19), 4446-4453
- Toutain, J. P., Baurbon, J. C.: Gas geochemistry and seismotectonics: a review. *Tectonophysics* 304, 1998. pp 1-24
- Truhlik, V., Benson, R.F., Fainberg, J., Osherovich, V., Yongli W., Bilitza, D., Fung, S.: Variation of the electron density in the high-latitude topside ionosphere during large magnetic storms, *General Assembly and Scientific Symposium, 2011 XXXth URSI*, doi: 10.1109/URSIGASS.2011.6051111
- Volland, H.: *Atmospheric Electrodynamics*. Heidelberg: Springer Verlag, 1984.

Wait, J. R.: Electromagnetic waves in stratified media. Pergamon Press, New York 1962.

Wernik, A.W., Wavelet transform of nonstationary ionospheric scintillation, Acta Geophys. Pol. 45, 1997, 237-253.

Wernik, A.W., Liu, C.H., Yeh, K.C.: Model computation of radio wave scintillation caused by equatorial ionospheric bubbles, Radio Sci. 15, 1980, pp. 559-572.

Wernik, A.W., Secan, J.A., Fremouw E.J.: Ionospheric irregularities and scintillation, Adv. Space Res. 31, 4, 2003, pp. 971-981.

Yoshida, M., Yamauchi, T., Horie, T., and Hayakawa, M. On the generation mechanism of terminator times in subionospheric VLF/LF propagation and its possible application to seismogenic effects. *Natural Hazards and Earth System Science*, Volume 8, Issue 1, 2008, pp.129-134

Yeh, K.C., Liu, C.H.: Radio wave scintillations in the ionosphere, Proc. IEEE 70, 1982, pp. 324-360.

Stochastic properties of lower ionosphere as earthquake precursor

Jan Šlégr · Kamila Váňová

Received: 28 October 2015 / Accepted: 14 April 2016
© Springer Science+Business Media Dordrecht 2016

Abstract Lower portion of the ionosphere known as the D-layer has properties of Gaussian random plane affecting very low frequency waves. This is manifested by stochastic properties of reflected VLF waves as their auto-correlation function (ACF) in time is the Bessel function of the first kind and zero order. In this paper, we show that the properties of this Bessel function are connected with the seismic activity in the area near the great circle path of VLF waves.

Keywords Earthquake prediction · Ionosphere · Auto-correlation

1 Introduction

It is well known that changes in the Earth's crust in the form of deformations, variations in seismic waves velocity, emanation of gases (King 1986) from the Earth's crust, changes in crustal electric conductivity, etc. affects the ionosphere. Several ionospheric precursors of earthquakes are currently under investigation (for details see Pulinets and Boyarchuk 2004

or Perrone et al. 2010), some of them using the VLF waves reflected by the ionosphere (Molchanov et al. 1998; Hayakawa et al. 2011). Electromagnetic precursors of earthquakes (not limited to VLF part of the electromagnetic spectrum) are discussed with case studied in recent monograph (Hayakawa 2015).

In this paper, we present novel method using the stochastic properties of reflected VLF waves.

2 Auto-correlation of reflected VLF signals

While for many years, ionosphere has been regarded as uniform, homogeneous, and regular-layered medium over short distances (e.g., Wait 1962), for long propagation multidiffraction, multireflection, and multiscattering effects are observed due to the formation of natural and artificial plasma structures (Blaunstein and Plohotniuc 2008, p. 127–138). Received wave then arrives at receiver via different propagation paths, thus the various components of the original wave arrive with different time delays and combine vectorially to give an oscillating signal.

Calculating the auto-correlation function of the received VLF signal, one gets Bessel function of the first kind and zero order. Typical result is depicted in the Fig. 1. For the automation of the data processing, the position of the first minimum of this Bessel function is studied (which is of course inversely proportional to the argument of the Bessel function).

J. Šlégr (✉) · K. Váňová
Department of Physics, University of Hradec Králové,
Náměstí Svobody 301, 500 02 Hradec Králové,
Czech Republic
e-mail: jan.slegr@uhk.cz

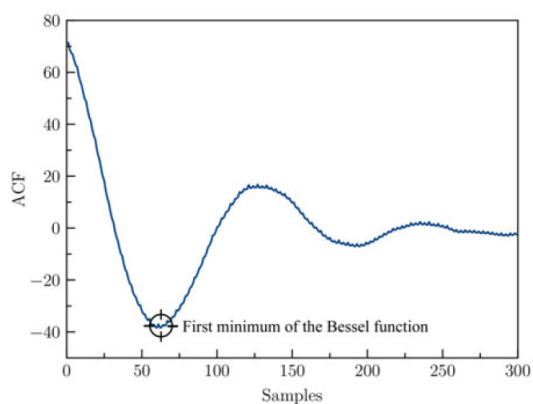


Fig. 1 Auto-correlation function of received VLF signal

3 Measuring technique

For the survey, the Denizköy VLF transmitter located in Turkey ($37^{\circ}24'43''N$ $27^{\circ}19'25''E$) active on 26700 Hz under the call-sign TBB was chosen. Two receivers were used, one in Czech Republic and one in France. The great circle paths of signal are shown in Fig. 2. This configuration was chosen to study earthquake precursors in the Mediterranean region, which is seismically active due to the northward convergence (4–10 mm/year) of the African plate with respect to the Eurasian plate along a complex plate boundary.

Very simple experimental setup was used to obtain field strengths. Loop antenna made of 20 turns of enameled wire was connected to the JFET pre-amplifier and NE5534 precision instrumental amplifier.

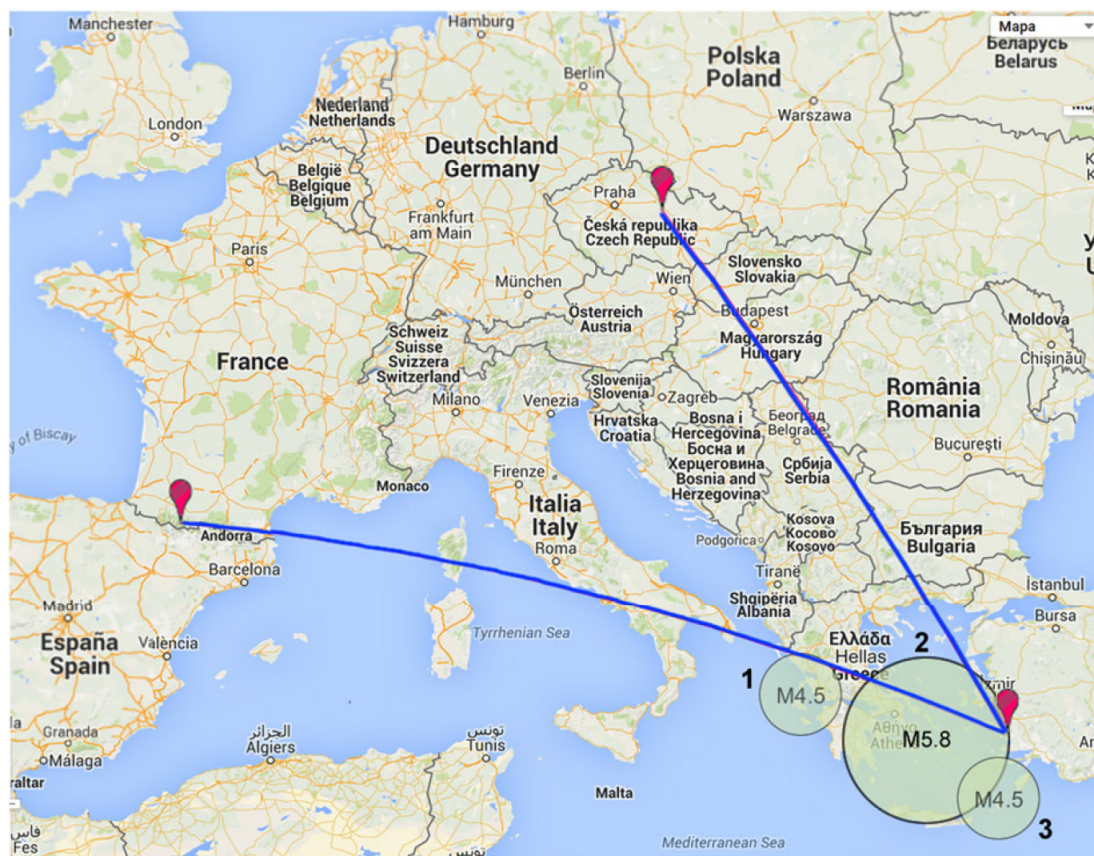


Fig. 2 Great circle paths of VLF waves from TBB transmitter with the preparation zones for three earthquakes (see text)

Amplified signal was fed to the sound card of an ordinary personal computer with a sampling frequency of 196 kHz. Sampling frequency of sound card is according to Shanon-Kotelnikovov theorem sufficient for VLF signals. 2^{16} -bin fast Fourier transformation was performed with custom software by Cooley-Tukey algorithm to obtain the frequencies of interest. Then the diurnal variation was subtracted from 24-h data and auto-correlation function was calculated using matlab.

4 Results

The auto-correlation function (ACF) minimum calculated for the 24-h data set is stable over several days and changes slowly through the year with maximal values around summer solstice and minimal around winter solstice. From this dependency, we can make assumption that the position of the first minimum of ACF is connected with the ionization of ionosphere. It is known that the ionization of the D-layer increases before earthquakes (Pulinets and Boyarchuk 2004).

Over 40 earthquakes with magnitude $M \geq 4.5$ were studied over the course of year. Typical results are shown in the Fig. 3. For M4.6 earthquake near Sami, Greece on 4 April 2015 at 04:38:20 UTC the ACF minimum position has evident deviation the day prior the earthquake. This earthquake with preparation zone of radius ~ 95 km (marked 1 in Fig. 2) was apparent in data received in France, not in the Czech Republic.

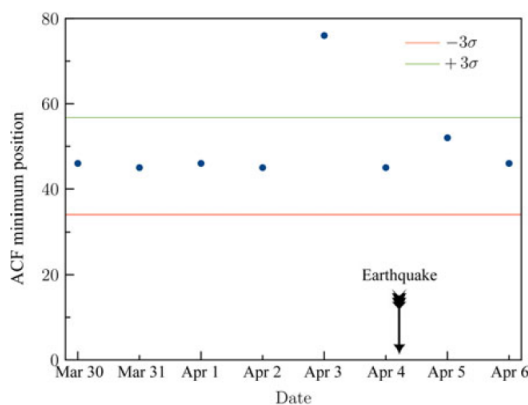


Fig. 3 Position of the first minimum of the ACF function before and after the M4.6 Sami earthquake

Figure 4 shows the ACF values for M5.6 earthquake near Adamas, Greece on 29 July 2015 at 03:45:06 UTC. This earthquake with preparation zone of radius ~ 310 km (marked 2 in Fig. 2) was apparent in data received both in France and Czech Republic. The average value of ACF is higher than for the Sami earthquake. That is caused by the fact that this earthquake was in summer. Despite the fact that this earthquake had greater magnitude, the deviation is not as prominent as in the case of the Sami earthquake. This effect was present in all the data and there is strong link between the depth of the epicenter and deviation in auto-correlation function (the Sami earthquake had epicenter in depth of 11 km, the Adamas in 80 km).

For earthquakes with preparation zones far from the great circle paths of VLF signals, no changes were observed (e.g., M4.5 earthquake near Palaikastron on 17 April 2015 at 16:39:42 UTC with epicenter depth of 27.8 km, marked 3 in Fig. 2). It seems that the radius ρ of the earthquake preparation zone calculated according to Dobrovolsky et al. (1979) as

$$\rho = 10^{0.43M} \text{ km},$$

where M is the magnitude, is a good clue to the estimation if the earthquake can be predicted with this method.

Data were investigated by calculating Pearson product-moment correlation coefficient for table with ACF minimum positions in one row and 1 or 0 (earthquake or no earthquake) in the second. For all earthquakes in selected region, no direct correlation

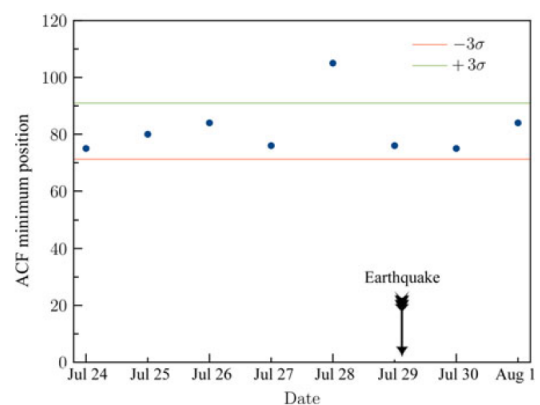


Fig. 4 Position of the first minimum of the ACF function before and after the M5.6 Adamas earthquake

was found, but for earthquakes with preparation zones under VLF propagation path the Pearson correlation coefficient was calculated as 0.954. Using table of critical values for two-tailed test from Freund (1984), the significance level is better than $\alpha=0.02$.

Because the used method is similar to the observational techniques described in Hayakawa (2015), data were examined to also study the terminator effect. Normal terminator effect is associated with phase changes of received components of diffracted waves during sunrise and sunset, manifested by minima in received VLF signal diurnal variation (both for the amplitude and phase). ‘‘Anomalous’’ terminator effect, described for example in Yoshida et al. (2008), is shift in this terminator times (in which the received wave amplitude or phase is minimal) the day or days prior the earthquake. This effect was observed for M6.0+ earthquakes and is not present in data from TBB transmitter studied in this paper. This was tested by calculating ACF minimum position for 10-min samples during the day and checking their behaviour for days before and after the earthquake. It was found that these values are well correlated (average Pearson’s correlation coefficient is around 0.7 for consecutive days) and no significant changes were found for days prior the earthquake. It was noted that these samples had higher values the day before earthquake, which is not surprising, because the overall value calculated from the whole 24-h data for day immediately before the earthquake have higher value of ACF minima position than for the other days. What is interesting is the fact that the values during the time when the Sun is above the horizon show nearly the same values of ACF minima position and the main difference (higher values) occurs at night. This is caused by the behavior of the ionosphere at night, when its ionization is not affected by radiation from the Sun.

5 Proposed explanation

The integral representation of Bessel function of the first kind and zero order is according to Stuber (1996)

$$J_0(x) = \frac{1}{2\pi} \int_{-\pi}^{\pi} e^{ix \sin t} dt.$$

If we assume the signal strength at the antenna as result of the superposition of (for simplicity) two plane

waves of the same frequency, one of them reflected from the ionosphere so that the two copies have angular separation θ . Then their correlation would vary like $e^{ix \cos \theta}$, because the projection of the wavelength of the reflected wave along the direction of its propagation of the other gets multiplied by $\cos \theta$. Now we can treat θ as a random variable distributed uniformly over the circle and compute the average. Thus, the Bessel function emerges as a consequence of the underlying geometry.

Ionosphere is very dynamic medium and the ionospheric scintillation emerges as result of continual electron density fluctuation ΔN . Signal scattering in random media was studied extensively and stochastic properties of signals propagation through random irregular electron density structures is treated extensively in Kung and Chao-Han (1982).

If we assume that an irregularity slab in the ionosphere can be characterized by a dielectric permittivity

$$\epsilon = \langle \epsilon_1 \rangle [1 + \epsilon_1(\mathbf{r}, t)],$$

where $\langle \epsilon_1 \rangle$ is the background average dielectric permittivity which for ionosphere is given by

$$\langle \epsilon_1 \rangle = (1 - f_{p0}^2/f^2)\epsilon_0$$

and $\epsilon_1(\mathbf{r}, t)$ is the fluctuating part characterizing the random variations in the ionosphere caused by the random irregularities and is given by

$$\epsilon_1(\mathbf{r}, t) = \frac{(f_{p0}/f)^2 [\Delta N(\mathbf{r}, t)/N_0]}{1 - f_{p0}^2/f^2}.$$

Here, f_{p0} is the plasma frequency corresponding to the background electron density N_0 and f is the frequency of the incident wave. If the percentage fluctuation $\Delta N/N_0 = 5$, the temporal variations, caused by the motion of irregularities, are assumed to be much slower than the period of the incident wave.

As the wave propagates through the irregularity slab, only the phase is affected by the random fluctuations in refractive index (to the first order). This phase deviation is equal to $k_0(\Delta\phi)$, where k_0 is the free space wave-number and $\Delta\phi$ is the optical path fluctuation:

$$\Delta\phi(\boldsymbol{\rho}) = -\frac{e^2}{2m\epsilon_0\omega^2} \Delta N_T(\boldsymbol{\rho}) = -\frac{\lambda^2}{2\pi} r_e \Delta N_T(\boldsymbol{\rho}),$$

where e is the electronic charge, m is its mass, ω is the circular radio frequency, r_e is the classical electron

radius and $\rho = (x, y)$ is the transverse coordinate. The deviation in the total electron content defined by

$$\Delta N_T(\rho) = \int \Delta N(\rho, z) dz.$$

Therefore, after the wave has emerged from the random slab, its phase front is randomly modulated. As this wave propagates to the ground, the distorted wave front will set up an interference pattern resulting in amplitude fluctuations.

It should be noted that other phenomena also play a role in scattering process: According to Stuber (1996) and with after-mentioned assumption of uniform distribution of θ over $[-\pi, \pi]$, we can write for the auto-correlation function

$$ACF = \frac{1}{2\pi} \int_{-\pi}^{\pi} \cos(2\pi f_d t \cos \theta) d\theta = J_0(2\pi f_d t),$$

where $J_0(x)$ is the modified Bessel function of the first kind and is zero-order. In the case of VLF waves scattered by ionosphere, there is no Doppler shift caused by motion of the transmitter or receiver, but there are small effects due to radial motion of the plasma (Saxton and Smith 1989), which are of order of 0.1 Hz. Nonlinear electron cyclotron resonance interaction near equator can also cause substantial changes in frequency and phase of the received signal (Clilverd et al. 2001). The position of the first minimum of the Bessel function then should be proportional to the constant $2\pi f_d$.

The penetration of electric field of seismic source into the plasmasphere causes formation of a VLF duct. This so called “seismic Trimpf-effect” was first proposed by Fishkova et al. (1985). Inside this duct cyclotron-resonance interaction between waves and particles leads to precipitation of energetic electrons into the lower atmosphere, finally leading to the increase in electron density in the ionospheric D-region (details of this mechanism can be found in Pulinets and Boyarchuk 2004). It was proposed that the additional electric field in the ionosphere cause the electric currents and turbulence. Hegai et al. (1997) calculated that for sufficiently strong electric field of short duration very anisotropic disturbances emerge with much longer duration than primary pulse of the electric field.

6 Other dynamic phenomena that could influence ACF

As it was previously stated, ionosphere is very dynamic medium. Other physical phenomena not related to earthquakes can change the properties governing the scattering of VLF waves. Impact of these processes must be ruled out. Two main influences have been taken into account:

6.1 Solar flares

It is well known that ionization of the lower ionosphere can increase considerably during chromospheric flares on the Sun as the X-ray and UV part of the solar spectrum penetrates the D-layer and the VLF wave strength during such a flare can either increase or decrease due to changes in the geometry of propagation. These density variations are different for different altitudes and are called Sudden Ionospheric Disturbances, SIDs. Details can be found for example in Mitra (1974) or Davies (1990).

Extensive statistical study of significant solar flares (up to X1.6 level, influencing the TBB transmitter signals during the survey period) showed that these flares had statistically negligible ($\alpha=0.05$) influence on ACF function computed over 24-h period.

6.2 Magnetic storms

During the magnetic storm main phase, relativistic electrons (with energies higher than 1 MeV) can precipitate from the plasma-pause to ionosphere, altering its conductivity due to changes in electron density (details can be found for example in Thorne and Kennel 1971). These changes can affect the received VLF signal amplitude. According to Demirkol et al. (1999), the VLF response is largely due to 100–300 keV electrons that accompany the 2–5 MeV electrons that signify relativistic electron enhancement events, because these are the particles which produce most of the ionization enhancement in the D-region where the VLF waves reflect.

This ionospheric effects are observed only when the electron flux is above 3×10^3 electrons/cm² · sr · s, apparently because of the fact that the VLF signature of the enhancement for lower fluxes is suppressed by other ionospheric variations.

These effects have to be taken into account for strong geomagnetic storms, but these events evolve on the longer time scales than are the oscillations of the VLF signal amplitude.

7 Conclusion

The correlation between the position of the first minimum of ACF and seismic activity in earthquake preparation zone was proven on significance level better than $\alpha=0.02$. This deviation is higher for the shallow earthquakes. Theoretical explanation of the phenomenon is proposed taking into account the penetration of the anomalous electric field into the ionosphere leading to increased ionization of the D-region.

This method has the same advantages as other VLF techniques described in Hayakawa (2015)—simple equipment and data processing. It was shown that for shallow earthquakes the threshold magnitude is around 4.5 for earthquakes with preparation zone under the great circle path of VLF signal. The main disadvantage is that this method cannot be used to predict earthquakes with deeper epicentres.

Acknowledgments This work was supported by the SV PpF UHK nr. 2119/2015.

References

- Blaunstein N, Plohotniuc E (2008) Ionosphere and applied aspects of radio communication and radar. CRC Press. Print ISBN: 978-1-4200-5514-6
- Cilverd MA, Rodger CJ, Thomson NR, Yearby KH (2001) Investigating the possible association between thunderclouds and plasmaspheric ducts. *J Geophys Res* 106(A12):29771–29781
- Davies K (1990) Ionospheric radio. Peter Peregrinus, London, p 580
- Demirkol MK, Inan US, Bell TF, Kanekal SG, Wilkinson DC (1999) Ionospheric effects of relativistic electron enhancement events. *Geophys Res Lett* 26(23):3557–3560. doi:10.1029/1999GL010686
- Dobrovolsky IR, Zubkov SI, Myachkin VI (1979) Estimation of the size of earthquake preparation zones. *Pageoph* 117:1025–1044
- Fishkova LM, Gokhberg MB, Pilipenko VA (1985) Relationship between night airglow and seismic activity. *Annal Geophys* 3:689–694
- Freund JE (1984) Modern elementary statistics. Prentice-Hall, Englewood Cliffs
- Hayakawa M (2015) Earthquake prediction with radio techniques. Wiley. doi:10.1002/9781118770368.ch1
- Hayakawa M, Raulin JR, Kasahara Y, Bertoni FCP, Hobara Y, Guevara-Day W (2011) Ionospheric perturbations in possible association with the 2010 Haiti earthquake as based on medium-distance sub ionospheric VLF propagation data. *Nat Hazard Earth Syst Sci* 11:513
- Hegai VV, Kim VP, Nikiforova LI (1997) A possible generation mechanism of acoustic-gravity waves in the ionosphere before strong earthquake. *J Earthquake Predict Res* 6:584–589
- King CY (1986) Gas geochemistry applied to earthquake prediction: an overview. *J Geophys Res* 91:12269
- Kung CY, Chao-Han L (1982) Radio wave scintillations in the ionosphere. *Proc IEEE* 70(4):324–360. doi:10.1109/PROC.1982.12313
- Mitra AP (1974) Ionospheric effects of solar flares. D. Reidel, Norwell, p 249
- Molchanov OA, Hayakawa M, Oudoh T, Kawai E (1998) Precursory effect in the sub-ionospheric VLF signals for the Kobe earthquake. *Phys Earth Planet Inter* 105: 239
- Perrone L, Korsunova LP, Mikhailov AV (2010) Ionospheric precursors for crustal earthquakes in Italy. *Ann. Geophys* 28:941–950. doi:10.5194/angeo-28-941-2010
- Pulinets S, Boyarchuk K (2004) Ionospheric Precursors of Earthquakes. Springer Verlag Publisher. ISBN: 978-3540208396
- Saxton JM, Smith AJ (1989) Quiet time plasmaspheric electric fields and plasmasphere-ionosphere coupling fluxes at $L = 2.5$. *Planet Space Sci* 37:283–293
- Stuber GL (1996) Principles of mobile communication. Kluwer Academic, Boston. ISBN: 0792397320
- Thorne RM, Kennel CF (1971) Relativistic electron precipitation during magnetic storm main phase. *J Geophys Res* 76(19):4446–4453. doi:10.1029/JA076i019p04446
- Wait JR (1962) Electromagnetic waves in stratified media. Pergamon Press, New York
- Yoshida M, Yamauchi T, Horie T, Hayakawa M (2008) On the generation mechanism of terminator times in subionospheric VLF/LF propagation and its possible application to seismogenic effects. *Nat Hazards Earth Syst Sci* 8(1):129–134